

# Unified model for fully and partially FRP confined circular and square concrete columns subjected to axial compression

Javad Shayanfar<sup>a,\*</sup>, Joaquim A. Barros<sup>a</sup>, Mohammadali Rezazadeh<sup>b</sup>

<sup>a</sup> Department of Civil Engineering, University of Minho, Azurém 4800-058 Guimarães, Portugal

<sup>b</sup> Civil Eng., Department of Mechanical and Construction Engineering, Northumbria University, Newcastle upon Tyne NE1 8ST, United Kingdom

## ARTICLE INFO

### Keywords:

FRP confined concrete  
Full confinement  
Partial confinement  
Square section  
Unified model

## ABSTRACT

Even though the usage of Fiber-reinforced polymer (FRP) full confinement arrangement is a more reliable and efficient strengthening technique than a partially confining strategy, it might not be cost-effective in real cases of strengthening. Experimental researches have demonstrated that confinement strengthening strategy is more effective for the case of circular columns compared to its application on square columns. This paper is dedicated to introducing a new unified model for determining the concrete confinement characteristics of FRP fully/partially confined circular/square concrete columns subjected to axial compressive loading. Through unification, the variations of the key parameters can be evaluated more-widely based on a unified mathematical framework. Consequently, it leads to the continuity in the predictions of FRP confinement-induced improvements for the different types of columns, contrary to those obtained from models only applicable to a specified cross-section or confining system. The substantial influence of non-homogenous concrete expansion distribution at the horizontal and vertical directions is taken into account in the determination of confinement pressure, besides arching action, by following the concept of confinement efficiency factor. Since the confinement-induced improvement is a function of its confining stress path, a new methodology is proposed to predict global axial stress–strain relation of FRP confined concrete columns considering confinement path effect, based on an extensive set of experimental results including 418 test specimens. The predictive performance of the developed model is assessed by simulating experimental tests reported in the literature.

## 1. Introduction

The strengthening of reinforced concrete (RC) columns by applying externally bonded fiber-reinforced polymer (FRP) is a well-established concept, that experimental research has demonstrated to be capable of increasing remarkably the axial compressive strength of these structural members, as well as their deformability without significant loss of load-carrying capacity. Campione *et al.* [1] examined experimentally the efficiency of a confinement strategy for improving the axial behavior of FRP fully confined circular concrete elements (FFCC as shown in Fig. 1). It was demonstrated that the effectiveness of this technique noticeably depends on FRP reinforcement ratio and, subsequently, FRP thickness and number of layers. Eid *et al.* [2] highlighted that the improvement in the axial strength and strain capacity is more pronounced in the case of FFCC with normal-strength concrete, compared to high-strength concrete.

Zeng *et al.* [3] conducted an experimental study to examine axial and

dilation behavior of FRP partially confined circular concrete elements (FPCC as shown in Fig. 1) with various confinement configurations. It was verified that the clear distance between FRP strips ( $s_f$ ) plays a key role in the establishment of axial and dilation responses, which was also experimentally confirmed by Barros and Ferreira [4] and Guo *et al.* [5].

It is well-established that in case of non-circular columns, the efficiency of confinement strategy is much smaller compared to circular columns, being this loss of effectiveness dependent on the corner radius,  $r$  ([6–8]). Wang and Wu [9] and Shan *et al.* [10] experimentally investigated the impact of the corner radius ratio,  $R_b = 2r/b$  (where  $b$  is the side of the section), on the axial response of FRP fully confined square cross-section concrete columns (FFSC as shown in Fig. 1). It was evidenced that decreasing  $R_b$  from one (circular section) to zero (square section with sharp edge), the confinement-induced improvements tended to be negligible. Likewise, Tao *et al.* [11] and Saleem *et al.* [12] experimentally verified that FRP thickness-induced improvements is a main function of  $R_b$ , so that it would be marginal for low value  $R_b$ . Triantafyllou *et al.* [13] and Zeng *et al.* [14] experimentally demonstrated

\* Corresponding author.

E-mail addresses: [id8287@alunos.uminho.pt](mailto:id8287@alunos.uminho.pt) (J. Shayanfar), [barros@civil.uminho.pt](mailto:barros@civil.uminho.pt) (J.A. Barros), [mohammadali.rezazadeh@northumbria.ac.uk](mailto:mohammadali.rezazadeh@northumbria.ac.uk) (M. Rezazadeh).

Nomenclature			
$A_{eff}$	Area of effective confinement zone	$k_{\epsilon, \min}$	Minimum value of $k_{\epsilon}^{FFSC}$
$A_g$	Total area of square cross-section columns	$N$	Total number of the fitted points
$A_{tot}$	Area of square cross-section	$n$	Concrete brittleness
$b$	Section dimension	$n_f$	FRP layer number
$D$	Diameter of circular column	$p_{tot}$	Perimeter of square cross-section
$D_{eq}$	Equivalent circular cross-section	$R_1$	Non-dimensional calibration coefficient
$D_{eq,c}$	Equivalent circular core	$R_2$	Non-dimensional calibration coefficient
$E_c$	Concrete modulus elasticity	$R_b$	Non-dimensional parameter as $2r/b$
$E_f$	FRP modulus elasticity	$R_f$	Non-dimensional parameter as $s_f/D_{eq}$
$f_c$	Axial stress corresponding to $\epsilon_c$	$r$	Corner radius
$f_{c0}$	Peak compressive stress of unconfined concrete	$s_f$	Distance between FRP strips
$f_{cc}$	Peak axial stress of FFSC/FPSC	$t_f$	FRP thickness
$f_f(z)$	FRP confining stress	$L$	Column height
$f_f^*$	Uniform FRP confining stress	$L_d$	Damage zone length of FRP confined concrete
$\hat{f}_{i,eff}$	Effective confinement pressure	$L_{d0}$	Damage zone length of unconfined concrete
$f_{i,f}^I$	Highest FRP confinement pressure	$V_{FRP}$	Volume of FRP jacket
$f_{i,f}^{II}$	Moderate FRP confinement pressure	$V_{con}$	Volume of concrete
$f_{i,f}^{III}$	Lowest FRP confinement pressure	$w_f$	FRP width
$f_{i,f}^{FFSC}$	FRP confinement pressure for FFSC	$\alpha_{\epsilon c}$	Ratio of $v_s$ and $v_{s,max}$
$f_{i,f}^{FPSC}$	Uniform FRP confinement pressure for FPSC	$\epsilon_c$	Axial strain corresponding to $f_c$
$f_{i,f}^{*FFSC}$	Uniform FRP confinement pressure for FFSC	$\epsilon_{c0}$	Axial strain corresponding to $f_{c0}$
$f_{i,f}^{*FPSC}$	Uniform FRP confinement pressure for FPSC	$\epsilon_{c,m}$	Axial strain corresponding to $v_{s,max}$
$\hat{f}_{i,i}$	Confinement pressure at strip mid-plane	$\epsilon_{cc}$	Axial strain corresponding to $f_{cc}$
$f_{i,j}$	Confinement pressure at the critical section	$\epsilon_h(z)$	Hoop strain
$h$	Longer side of section	$\epsilon_{h,c}$	Hoop strain at the corners
$I_f$	Confinement stiffness index	$\epsilon_{h,m}$	hoop strain at the middle of the flat side
$I_f^*$	Confinement stiffness index leading to $v_{s,max} = 0.5$	$\epsilon_{h,max}$	Maximum FRP hoop strain
$K_e$	Confinement efficiency factor	$\epsilon_{h,min}$	Minimum FRP hoop strain
$k_{ff}^{FFSC}$	Reduction factor $k_{ff}$ for FFSC	$\epsilon_l(z)$	Concrete lateral strain
$k_{ff}^{FPSC}$	Reduction factor $k_{ff}$ for FPSC	$\epsilon_{l,i}$	Concrete expansion at the mid-plane of FRP strips
$k_{h,f}$	Reduction factor	$\epsilon_{l,j}$	Lateral concrete expansion at the critical section
$k_{h,eff}$	Reduction factor	$\epsilon_V$	Volumetric strain
$k_{v,f}$	Reduction factor	$\rho_f$	FRP volumetric ratio
$k_{\epsilon}^{FFSC}$	Reduction factor for FFSC	$\rho_{f,eq}$	Equivalent FRP volumetric ratio
$k_{\epsilon}^{FPSC}$	Reduction factor for FPSC	$\rho_{K,f}$	FRP confinement stiffness index
$k_{\epsilon h}$	Reduction factor	$v_s$	Secant Poisson's ratio
		$v_{s,0}$	Initial Poisson's ratio of unconfined concrete
		$v_{s,max}$	Maximum Poisson's ratio at the critical section

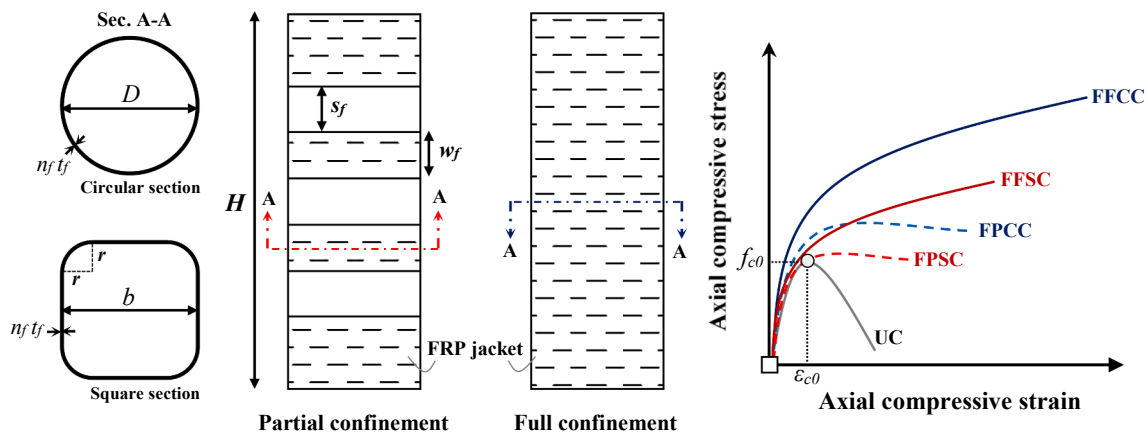


Fig. 1. Various confinement configurations. Note: UC: unconfined concrete column; FFCC: FRP fully confined circular concrete column; FPCC: FRP partially confined circular concrete column; FFSC: FRP fully confined square concrete column; FPSC: FRP partially confined square concrete column;

that the effectiveness of FRP partially confined square concrete columns (FPSC as shown in Fig. 1) is directly dependent on the spacing of the strips of FRP sheets,  $s_f$ , being their axial and dilation behavior

detrimentally affected with the increase of  $s_f$  due to concrete damage concentration in the zones between strips.

Even though the usage of FRP full confinement arrangement (FFCC

and FFSC) is a more reliable and efficient strengthening technique than partially confining strategy (FPCC and FPSC), it might not be cost-effective in the real cases of strengthening, considering the relatively high cost of FRP materials. The studies [4,13,14] experimentally revealed that the application of discontinuous FRP wrapping strips in non-seismically designed RC columns would be able to offer a reliable compromise between confinement-induced improvements and cost competitiveness, under proper design circumstances. In order to predict FRP confinement-induced improvements, numerous models have been recommended in the literature (i.e. [15–24]). Conventionally, for the establishment of the axial response of FFCC, at a certain axial strain leading to a specific confinement pressure, FRP confinement-induced improvements are assumed to be identical to that of actively-confined concrete (AFCC) where concrete is subjected to a constant lateral pressure during the entire axial loading (Lam and Teng [15]). According to this assumption, at a certain level of axial strain generating a specific confinement pressure, the corresponding axial stress of FFCC can be derived using the axial stress–strain base framework suggested for AFCC (i.e. Popovics [25]) by considering identical confinement-induced improvements for FFCC and the corresponding AFCC subjected to the same lateral confinement pressure. However, Lim and Ozbakkaloglu [20,26,27] evidenced an imperative difference in terms of axial and dilation behavior, generally known as confinement path effect, in enhancements offered by FRP jacketing (FFCC) and active confinement. It was evidenced that axial stress–strain relationship, conventionally determined, would result in misleading prediction in terms of axial capacity of FFCC, as also confirmed by Yang and Feng [22] and Lin *et al.* [23]. Lim and Ozbakkaloglu [20] refined this assumption by suggesting a reduction factor in actual FRP confinement pressure to reduce confinement-induced improvements imposed by active confinement for taking into account confinement path effect in the case of FFCC. For the same purpose, Yang and Feng [22] presented a refined version of the original assumption by considering the confinement path effect in the prediction of FRP confinement-induced improvements during axial loading based on the actual FRP confinement pressure.

For the establishment of axial stress–strain response of FFSC, in general, the concept of confinement efficiency factor, originally developed by Mander *et al.* [28] for the case of steel confined concrete with stirrups is adopted (i.e. Guo *et al.* [29]), which formulates the detrimental influence of horizontal arching action as a reduction factor in confinement pressure. In this approach, based on the effectiveness of confinement pressure acting on the non-circular concrete section columns, the concrete regions are classified in two distinct zones as, so-called, effective confinement area and ineffective confinement area. The former is assumed to be homogeneously/effectively mobilized by confinement pressure, while the latter is assumed to be as unconfined concrete. However, the finite element simulations performed by [30–33] demonstrated that the effective confinement area is subjected to a non-uniform distribution of confinement pressure, which strongly depends on the length of corner radius. Furthermore, the studies [6,7,32,33] experimentally evidenced that FRP hoop strain at the horizontal direction is non-homogeneously distributed in the perimeter, in contrary to what happens in circular sections. On the other hand, for the establishment of axial stress–strain response of FPCC, the concept of confinement efficiency factor is also adopted by addressing the effect of vertical arching action (and horizontal arching action effect in case of FPSC) in the determination of confinement pressure imposed by FRP strips. Zeng *et al.* [34] experimentally evidenced the distribution of concrete expansion would be predominantly non-homogenous, particularly in the case of large  $s_f$ , as also confirmed by Guo *et al.* [29]. Likewise, Zeng *et al.* [14] and Guo *et al.* [5,29] evidenced the non-uniform distribution of concrete expansion of FPCC and FPSC, so that by decreasing  $s_f$  the dilation behavior changed from being localized to be more homogenous. Accordingly, Shayanfar *et al.* [35] suggested a refined version of the concept of confinement efficiency factor for FPCC by formulating not only the influence of vertical arching action but also

the non-homogenous concrete lateral expansibility in generating confining stress.

Nonetheless, the development of a confinement model applicable to FFCC, FFSC, FPCC and FPSC, by addressing the influences of confinement path, vertical and horizontal arching action, and the non-homogenous confining stress/strain distributions at the longitudinal and transverse directions in the prediction of confinement-induced improvement, is still lacking. It should be noted that unification of the models for concrete columns fully and partially confined with FRP systems (FF and FP) as well as for the case of circular and square cross-sections (CC and SC) can be achieved through the concept of confinement efficiency factor. Such unification does not lead to discontinuity between the estimations of FRP confinement-induced improvements for the cases of FF and FP when  $s_f$  approaches to nearly zero (i.e. closely spaced FRP partial strips) and the cases of CC and SC when  $R_b$  ( $2r/b$ ) approaches to almost 1. Next, the range and variations of the key parameters as well as their interactions can be simulated more-widely based on a unified mathematical framework. This provision in the establishment of the confinement model, which is unavoidably based on regression analysis technique, would lead to a more-reliable predictive performance, compared to the case where a limited variation for the key parameters is assumed.

In the present study, a new unified model is proposed for estimating the behavior of concrete columns of circular and square cross-sections (CC and SC) full and partially confined with FRP systems (FF and FP). By following a unified approach with FFCC and FPCC, the concept of the equivalent circular section is presented for the cases of FFSC and FPSC. For simulating the effect of concrete expansion distribution at the horizontal and vertical directions, an extended version of the model recommended by Shayanfar *et al.* [35] is developed. Based on an extensive set of experimental results including 418 test specimens, a new unified analysis-oriented model in compliance with the concept of the confinement efficiency factor is introduced to predict the axial response of FRP confined concrete columns. Lastly, the predictive performance of the developed confinement model is assessed through analytically simulating experimental results of FFCC, FPCC, FFSC and FPSC.

## 2. Concept of equivalent circular Cross-section

Numerous analysis-oriented models have been developed to predict the confinement-induced improvements of FRP confined circular cross-section columns during axial concentric loading. For simulating the FRP confinement effects on concrete columns of square cross-section, the possibility of considering this type of column as an equivalent circular column is very attractive due to the consequent simplification obtained for the corresponding formulation. In this regard, equivalent diameter concept has been proposed by several researchers ([15,18,36–38]). In these models, the diameter of the equivalent circular cross-section ( $D_{eq}$ ) has been suggested based on (i) Diagonal length of the cross-section, and (ii) FRP volumetric ratio, as the ratio of the volume of FRP and concrete. In the former group, Lam and Teng [15] recommended  $D_{eq}$  equal to the diagonal length of the section ( $D_{eq} = \sqrt{h^2 + b^2}$ ), where  $h$  and  $b$  are the length of the longer and shorter sides of the section, respectively. In this group, for the case of square section, it would be as  $D_{eq} = \sqrt{2}b$ , regardless of the dimension of corner radius. By improving this model in order to consider the effect of rounded corners, Lee *et al.* [18] suggested  $D_{eq}$  as the diagonal distance from the centers of two corner arcs as  $D_{eq} = \sqrt{2}(b - 2r) + 2r$ . In the latter group,  $D_{eq}$  is determined so that the equivalent FRP volumetric ratio ( $\rho_{f,eq}$ ) of non-circular column could be the same of  $\rho_f$  in square columns. Triantafillou *et al.* [38] adopted this approach for the case of rectangular columns as  $D_{eq} = 2bh/(b + h)$ . For the case of the square section, this model can be expressed as  $D_{eq} = b$ , regardless of the length of corner radius.

In the present study, for transforming a square cross-section in an equivalent circular section, the approach suggested by Triantafillou *et al.*

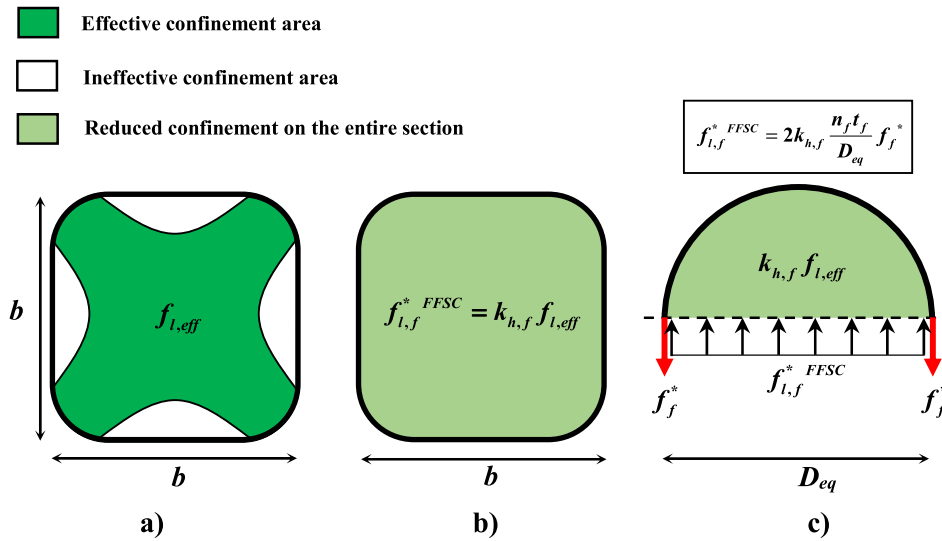


Fig. 2. Distribution of confinement pressure in FRP confined square column based on OCCEF.

[38] is adopted with a slight modification in terms of the consideration of corner radius in determining  $D_{eq}$ . This approach defines the equivalent circular section for square section based on its  $\rho_f$ , which is one of the key parameters in the establishment of the confinement pressure. Accordingly,  $\rho_{f,eq}$  for the equivalent circular column would be the same of  $\rho_f$  in square columns as:

$$\rho_f = \rho_{f,eq} \left( \frac{V_{FRP}}{V_{con}} \right)_{original} = \left( \frac{V_{FRP}}{V_{con}} \right)_{equivalent} \quad (1)$$

where  $V_{FRP}$  and  $V_{con}$  are the volume of FRP jacket and concrete, respectively. Rearranging Eq. (1) leads to

$$\frac{p_{tot}}{A_{tot}} \times n_f t_f = \frac{4n_f t_f}{D_{eq}} \quad (2)$$

where  $n_f$  and  $t_f$  are the FRP layer number and thickness;  $p_{tot}$  and  $A_{tot}$  are the perimeter and area of the square cross-section wrapped by FRP, respectively. Therefore, considering the impact of rounded corners,  $D_{eq}$  can be expressed using Eq. (2):

$$D_{eq} = 4 \times \frac{A_{tot}}{p_{tot}} = 4 \times \frac{b^2 - 4 \left( r^2 - \frac{\pi r^2}{4} \right)}{4(b - 2r) + 4 \frac{\pi r}{2}} = \frac{b^2 - 4r^2 + \pi r^2}{b - 2r + \frac{\pi r}{2}} \quad (3)$$

Rearranging the above equation gives:

$$D_{eq} = \frac{1 - 0.215R_b^2}{1 - 0.215R_b} b \quad (4)$$

in which

$$R_b = \frac{2r}{b} \quad (5)$$

Through employing Eq. (4), FRP volumetric ratio of the equivalent circular section would be the same as that of square section. Despite FRP volumetric ratio be a key parameter in the development of confinement pressure, the confinement-induced improvement also depends on the detrimental influence of the horizontal arching action, leading to a reduction in the confinement efficiency of non-circular columns, compared to circular columns. In order to formulate this effect, in general, the concept of ‘confinement efficiency factor’ is employed, which will be addressed in the following section.

### 3. Original concept of confinement efficiency factor

According to the original concept of ‘confinement efficiency factor’

(OCCEF), during axial compressive loading, concrete regions in the case of FFSC would be subjected to two different confinement levels, due to the arching action phenomena at the cross-sectional level. Based on the effectiveness of confinement pressure, for the sake of simplicity in the design context, the concrete regions are classified in two distinct areas due to arching action (Fig. 2a):

- i). Effective confinement area
- ii). Ineffective confinement area

In OCCEF, the former is assumed as homogeneously and effectively under the highest confinement pressure ( $f_{l,eff}$ ), while the latter is considered to be under the lowest confinement pressure, conservatively assumed as unconfined concrete. Through a reduction factor ( $k_{h,f}$ ), the effective confinement pressure ( $f_{l,eff}$ ) acting on the effective confined area is transformed in a homogeneously confining pressure on the entire cross-section ( $f_{l,f}^{*FFSC}$ ) as shown in Fig. 2b (the “\*” in the superscript aims to represent that the generated confinement pressure is distributed uniformly not only at the cross-sectional level, but also at the cross-sectional level). It can be expressed as:

$$f_{l,f}^{*FFSC} = k_{h,f} f_{l,eff} \quad (6)$$

Mander *et al.* [28] defined  $k_{h,f}$  as  $A_{eff}/A_g$ , where  $A_{eff}$  and  $A_g$  are the area of effective confinement zone and the area of the entire square cross-section, respectively. Consequently, by using the concept of the equivalent circular cross-section ( $D_{eq}$ ), based on the equilibrium of confinement forces,  $f_{l,f}^{*FFSC}$  corresponding to the FRP confining stress  $f_f^*$  (the “\*” in the superscript aims to represent that the distribution of confining stress in the cross-sectional perimeter of the equivalent circular cross-section is homogenous) can be determined by (Fig. 2c):

$$f_{l,f}^{*FFSC} = 2k_{h,f} \frac{n_f t_f}{D_{eq}} f_f^* \quad (7)$$

where  $n_f$  is the number of FRP layers;  $t_f$  is the thickness of a FRP layer;  $E_f$  is the FRP modulus of elasticity. Nevertheless, contrary to OCCEF, the finite element simulations performed by [30–33] well evidenced that the effective confined area is subjected to a non-uniform distribution of confinement pressure, which strongly depends on the dimension of the corner radius ( $R_b$ ). Fig. 3 demonstrates the distribution of confinement pressure in a quarter of the square cross-section column (FFSC) obtained from the finite element analyses performed by Jiang *et al.* [32] on FFSC specimens tested by [9]. As can be seen, due to the restriction imposed by the confining system, near the center of the cross-

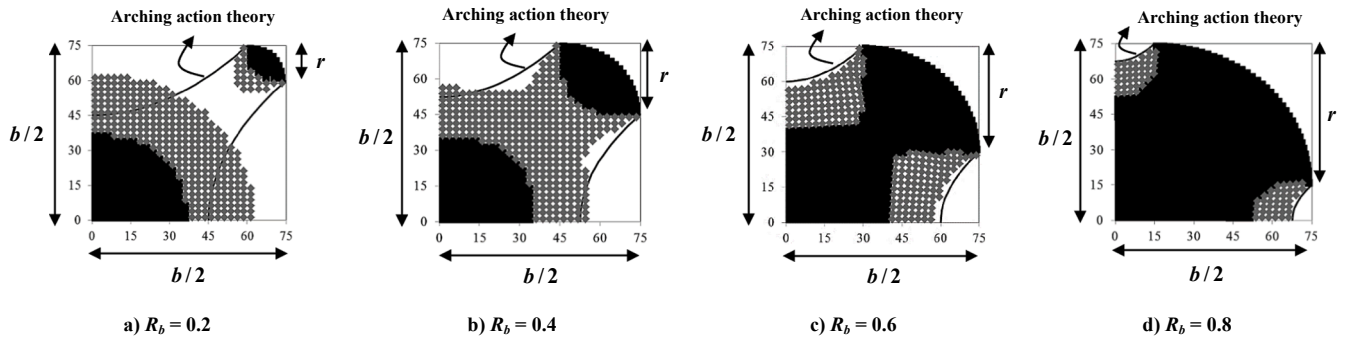


Fig. 3. Typical distribution of confinement pressure obtained from finite element simulations performed by [32] Note: White zone: associated with low confinement level; Gray zone: moderate confinement level; Black zone: high confinement level [32].

section and the corner areas are under the highest level of confinement pressure (black color). However, as a consequence of horizontal arching action, the concrete closer to the flat sides of the section is subjected to the lowest confinement pressure (white color). The zone between the well and less confined concrete regions can be regarded to be subjected to a moderate level of confinement pressure (gray color). By increasing the corner radius, the area of highly confined zone would be enlarged and the stress concentration at the corners is reduced. Likewise, for higher  $R_b$ , the confined concrete regions under low and moderate levels of confinement pressure are merged, and the section tends to be confined homogeneously. As a result, based on the demonstrated

confinement pressure distribution observed in the numerical simulations, three distinct concrete areas can be distinguished representing those subjected to lowest, moderate and highest confinement levels. Accordingly, a modified concept of the confinement efficiency factor (MCCEF) is, herein, proposed which is presented in the following section.

#### 4. Modified concept of confinement efficiency factor

It is noteworthy that the arching action theory demonstrated in Fig. 3 seems to be sufficient in separating the concrete with the lowest

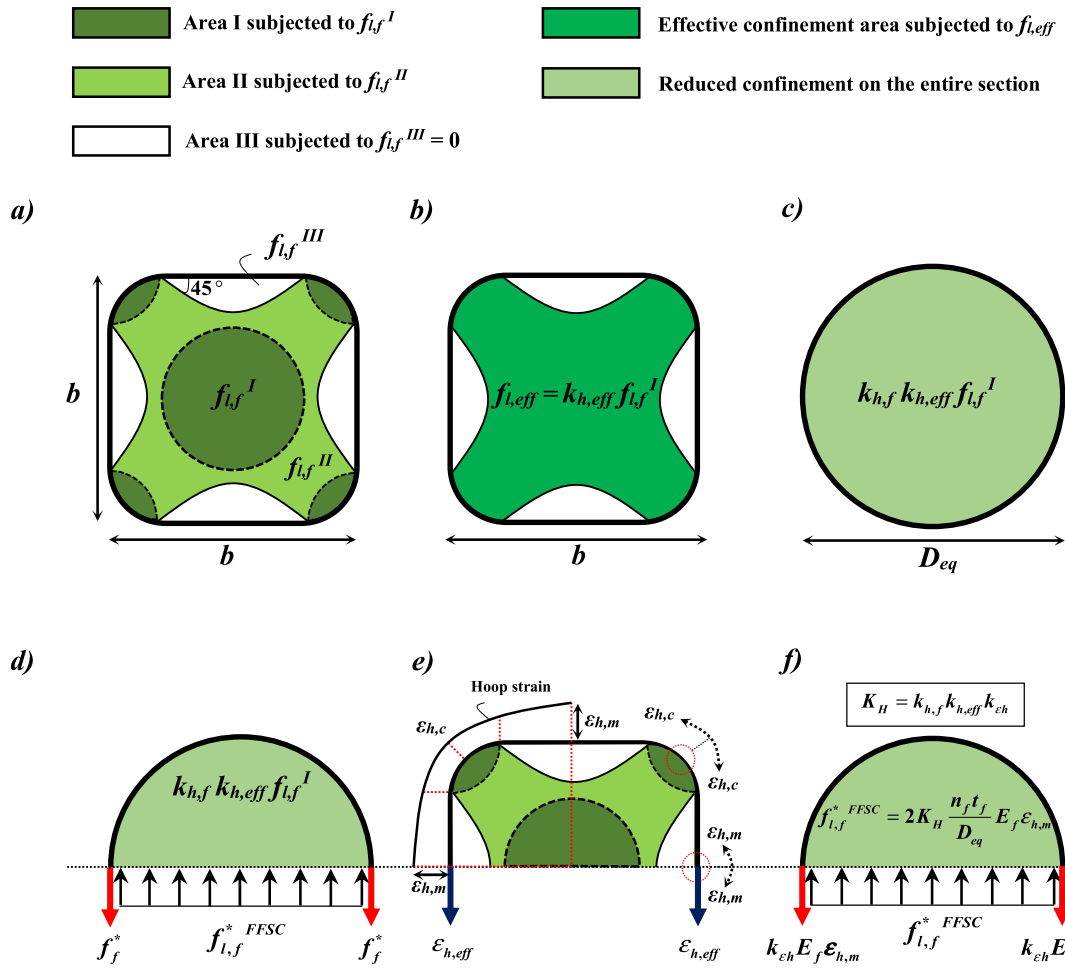


Fig. 4. Distribution of confinement pressure based on MCCEF.

confinement level (white color) from those under moderate and highest confinement levels, particularly for higher  $R_b$ . In MCCEF through adopting the arching action theory, the three concrete regions represented in Fig. 4a are distinguished according to the level of the confinement pressure level acting on these zones:

- i). Area I, subjected to the highest level of confinement pressure,  $f_{1f}^I$
- ii). Area II, confined, with a moderate level of confinement pressure  $f_{1f}^{II}$
- iii). Area III, with negligible confinement (the lowest confinement level), therefore  $f_{1f}^{III} = 0$  for the sake of simplicity.

To take into account the non-homogenous confinement pressure distribution in the effective confinement area contained by the parabolas, Area I and Area II under different confinement pressures were defined based on finite element simulations [32]. As shown in Fig. 4a, Area II subjected to  $f_{1f}^{II}$  is located between Area I and Area III under  $f_{1f}^I$  and  $f_{1f}^{III}$ , respectively. Accordingly, as the concrete is a non-homogenous continuous material, in Area II, for the concrete next to Area III,  $f_{1f}^{II} \simeq f_{1f}^{III}$ , while for the concrete next to Area I,  $f_{1f}^{II} \simeq f_{1f}^I$ . Therefore,  $f_{1f}^{II}$  can be considered between these extremities as  $f_{1f}^{III} \leq f_{1f}^{II} \leq f_{1f}^I$ . Considering  $f_{1f}^{III} = 0$  (OCCEF), it can be rearranged as  $0 \leq f_{1f}^{II} \leq f_{1f}^I$ . In the present study, in order to determine a weighted average level of confinement pressure acting on Area II, for the sake of simplicity and lack of adequate experimental/numerical investigations in the literature, a linear variation for the confinement pressure between these extremities was assumed, leading to  $f_{1f}^{II} = 0.5f_{1f}^I$ .

In MCCEF,  $f_{1,eff}$  is defined as the weighted average level of confinement pressure acting homogeneously on Area I and Area II, in the compliance with the effective confinement area in OCCEF. It can be considered on the interval  $[f_{1f}^{II}, f_{1f}^I]$  depending on  $R_b$ . Likewise,  $f_{1,eff}$  as a function of the highest confinement level ( $f_{1f}^I$ ) can be expressed as:

$$f_{1,eff} = k_{h,eff} f_{1f}^I \quad (8)$$

where  $k_{h,eff}$  ( $f_{1,eff}$  and  $f_{1f}^I$  ratio) is on the interval [0.5, 1]. As shown in Fig. 4b, by using  $k_{h,eff}$ , the non-homogenous confinement distribution can be converted into a reduced confinement pressure uniformly/effectively acting on the effective confinement area. This reduced confinement can be distributed on the entire cross-section through implementing the reduction factor  $k_{h,f}$  in the compliance with OCCEF (Fig. 4c). By putting Eq. (8) in Eq. (6), the equivalent confinement pressure of  $f_{1f}^{*FFSC}$  as a function of  $k_{h,f}$  and  $k_{h,eff}$  can be obtained as:

$$f_{1f}^{*FFSC} = k_{h,f} f_{1,eff} = k_{h,f} k_{h,eff} f_{1f}^I \quad (9)$$

Therefore, based on the equilibrium of confinement forces,  $f_{1f}^{*FFSC}$  corresponding to the FRP confining stress  $f_f^*$  can be derived as (Fig. 4d):

$$f_{1f}^{*FFSC} = 2k_{h,f} k_{h,eff} \frac{n_f t_f}{D_{eq}} f_f^* \quad (10)$$

Compared with OCCEF presented in Eq. (7), MCCEF contains the reduction factor of  $k_{h,eff}$  reflecting the effect of non-homogenous confinement pressure in the determination of  $f_{1f}^{*FFSC}$ . On the other hand, based on Eqs. (7,10),  $f_{1f}^{*FFSC}$  is in a direct proportion with FRP confining stress  $f_f^*$  generated in the perimeter of the equivalent circular cross-section. Nonetheless, as experimentally confirmed by Ozbakkaloglu [6], Chen and Ozbakkaloglu [7], Shan et al. [19] and Oliveira and Carrazedo [33], for a square section, at a certain axial strain ( $\epsilon_c$ ), the middle of the flat side would experience the maximum hoop strain in the perimeter ( $\epsilon_{h,max} = \epsilon_{h,m}$ ), but the minimum occurs at the corners ( $\epsilon_{h,min} = \epsilon_{h,c}$ ) as demonstrated in Fig. 4e. The extra strain at the middle of the flat

side can be attributed to i) the frictional effect where the frictional components in the corner zones induces a reduction in the strain of the FRP applied on this zone; ii) the transversal deformability of the concrete of the unconfined region (as ineffective confinement area shown in Fig. 3), iii) the bending effects in the FRP at flat sides considering its relatively low flexural stiffness, as experimentally confirmed (Wang and Wu [9] and Shan et al. [10]). Therefore, since the hoop strain distribution of the equivalent circular cross-section is homogenous, the effect of non-uniform distribution of hoop strain along the perimeter of a square section needs to be addressed in the establishment of FRP confining stress  $f_f^*$ . In the confinement models developed by Lee et al. [18] and Lin and Teng [24], the hoop confining strain at the corner centers ( $\epsilon_{h,c}$ ) was taken into account as the effective hoop strain ( $\epsilon_{h,eff}$ ), homogeneously distributed in the perimeter of FFSC, leading to FRP confining stress ( $f_f^*$ ) as  $E_f \epsilon_{h,eff}$  (Fig. 4e). Consequently, by defining  $k_{eh}$  as the ratio of  $\epsilon_{h,c}$  and  $\epsilon_{h,m}$ ,  $f_f^*$  can be expressed as:

$$f_f^* = E_f \epsilon_{h,eff} = E_f \epsilon_{h,c} = k_{eh} E_f \epsilon_{h,m} \quad (11)$$

Therefore, replacing Eq. (11) in Eq. (10) gives:

$$f_{1f}^{*FFSC} = 2k_{h,f} k_{h,eff} k_{eh} \frac{n_f t_f}{D_{eq}} E_f \epsilon_{h,m} = 2K_H \frac{n_f t_f}{D_{eq}} E_f \epsilon_{h,m} \quad (12)$$

in which

$$K_H = k_{eh} k_{h,f} k_{h,eff} \quad (13)$$

where  $K_H$  represents the efficiency confinement factor addressing the influence of horizontal arching action. Therefore, Eq. (12) provides the uniform confinement pressure  $f_{1f}^{*FFSC}$ , which is assumed to homogeneously act on the entire equivalent circular cross-section with  $D_{eq}$  through adopting the reduction factor  $K_H$ . For this purpose, the determination of  $k_{h,f}$ ,  $k_{h,eff}$  and  $k_{eh}$  as input parameters in Eq. (13) is essential, which will be addressed in the following sections.

#### 4.1. Determination of $k_{h,f}$

This section provides the formulation for determining  $k_{h,f}$  presenting the ratio of  $f_{1,eff}$  and  $f_{1f}^{*FFSC}$ , based on Eq. (6). Through applying this reduction factor,  $f_{1,eff}$  on the effective confinement area is spread homogeneously on the entire equivalent circular cross-section with  $D_{eq}$  as shown in Fig. 5a. In the figure, it was assumed that  $D_{eq,c}$  defines the diameter of equivalent circular core representing the effective confinement area (Area I and Area II). Consequently, the equilibrium of the generated confinement forces on the equivalent circular core ( $D_{eq,c}$ ) and the entire section ( $D_{eq}$ ) can be expressed as (Fig. 5a):

$$f_{1f}^{*FFSC} D_{eq} = f_{1,eff} D_{eq,c} \quad (14)$$

Thus, using Eq. (14),  $k_{h,f}$  is obtained as

$$k_{h,f} = \frac{f_{1,eff}}{f_{1f}^{*FFSC}} = \frac{D_{eq,c}}{D_{eq}} \quad (15)$$

in which  $D_{eq}$  is calculated by Eq. (4). Hence, to calculate  $k_{h,f}$ ,  $D_{eq,c}$  needs to be addressed. For this purpose, based on the concept of the equivalent circular section used to derive Eq. (4),  $D_{eq,c}$  can be determined as:

$$D_{eq,c} = 4 \times \frac{A_{eff}}{p_{eff}} = 4 \times \frac{A_{tot} - \sum A_{ine}}{2\pi r + \sum p_{ine}} \quad (16)$$

where  $p_{eff}$  and  $A_{eff}$  are the perimeter and area of the effective confinement area, respectively;  $\sum p_{ine}$  and  $\sum A_{ine}$  are the perimeter and area of the ineffective confinement zones, respectively; In the present study, as demonstrated in Fig. 5a, by considering the unconfined concrete due to arching action as defined by a second-degree parabola between the adjacent corners, the corresponding perimeter and area are

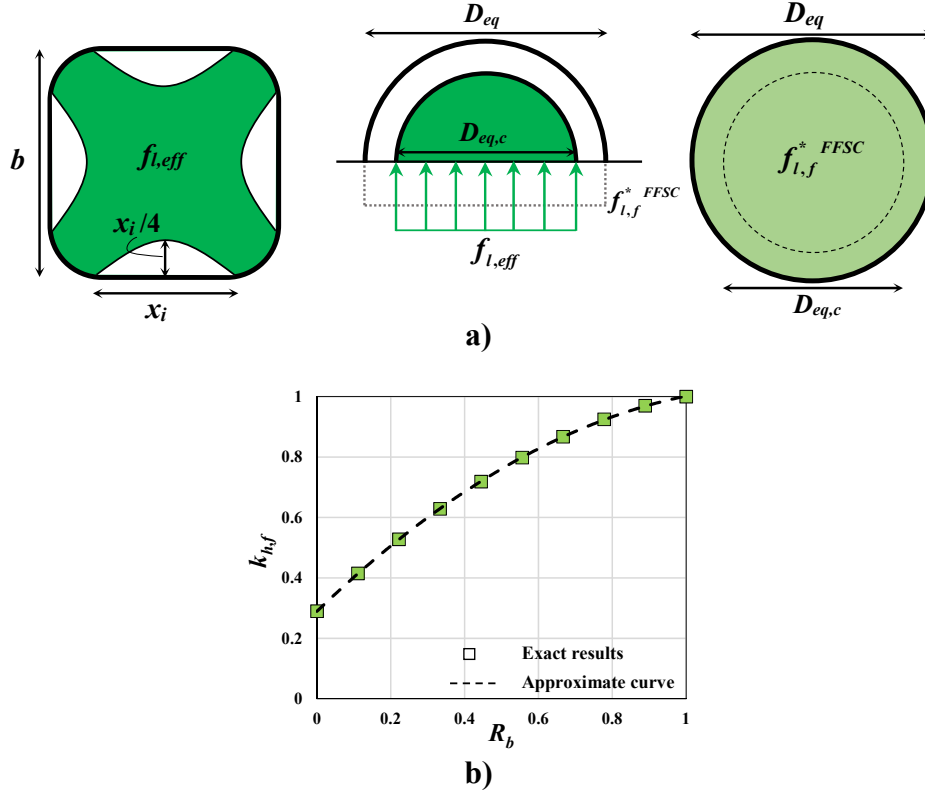


Fig. 5. (a) Arching action in FFSC; (b) Variation of  $k_{h,f}$  with respect to  $R_b$ .

calculated as  $p_{ine} = 2.3x_i$  and  $A_{ine} = 2x_i^2/3$ . The relative complexity of Eq. (16) was, in the present study, overcome by adopting a simplified equation. Accordingly, the best-fit  $k_{h,f}$  was derived using a regression analysis of the results obtained from Eq. (16) as:

$$k_{h,f} = 1.17R_b - 0.46R_b^2 + 0.29 \quad (17)$$

Fig. 5b shows that Eq. (17) fits with high accuracy the discrete results in terms of  $k_{h,f}$  versus  $R_b$  in the interval 0 to 1 for the  $R_b$  (note that for  $R_b = 1$ , circular cross-section,  $k_{h,f} = 1$ ).

#### 4.2. Determination of $k_{h,eff}$

This section provides the formulation for determining  $k_{h,eff}$  presenting the ratio of  $f_{l,eff}$  and  $f_{l,f}^I$ , based on Eq. (8). Using this factor, the non-uniform confinement distribution within Areas I and II is converted into  $f_{l,eff}$  as demonstrated in Fig. 4a-b. By transforming the confinement regions of Area I and II into two equivalent circular shapes with  $D_{eq}^I$  and  $D_{eq}^{II}$  respectively, the confinement force generated in each region can be determined as  $f_{l,f}^I D_{eq}^I$  and  $f_{l,f}^{II} D_{eq}^{II}$ . On the other hand, as demonstrated in the previous Section, the confinement force generated by  $f_{l,eff}$  acting on the effective confinement area is as  $f_{l,eff} D_{eq,c}$ . On the basis of the superposition principle,  $f_{l,eff} D_{eq,c}$  can be written through equality in  $f_{l,f}^I D_{eq}^I$  and  $f_{l,f}^{II} D_{eq}^{II}$ :

$$f_{l,eff} D_{eq,c} = f_{l,f}^I D_{eq}^I + f_{l,f}^{II} D_{eq}^{II} \quad (18)$$

By considering the assumption of  $f_{l,f}^{II} = 0.5f_{l,f}^I$ , rearranging Eq. (18) gives

$$f_{l,eff} = \frac{D_{eq}^I + 0.5D_{eq}^{II} f_{l,f}^I}{D_{eq,c}} \quad (19)$$

Accordingly, by using Eq. (19),  $k_{h,eff}$  can be determined as

$$k_{h,eff} = \frac{f_{l,eff}}{f_{l,f}^I} = \frac{D_{eq}^I + 0.5D_{eq}^{II}}{D_{eq,c}} \quad (20)$$

As obtained in Eq. (20),  $k_{h,eff}$  is a function of  $D_{eq}^I$  and  $D_{eq}^{II}$ , strongly depending on  $R_b$ . For the case of FFSC with relatively sharp corner ( $R_b \simeq 0$ ), Area I would become virtually marginal as numerically confirmed by [30–33]. Consequently, for  $R_b \simeq 0$ , by ignoring the contribution of ( $f_{l,f}^I$ ) acting on Area I in terms of  $f_{l,eff}$  ( $D_{eq}^I \simeq 0$ ), the entire effective confinement area (with  $D_{eq,c}$ ) can be assumed to be only under  $f_{l,f}^{II}$ , leading to  $D_{eq}^{II} \simeq D_{eq,c}$ . Thus,  $k_{h,eff} \simeq 0.5$  by using Eq. (20). Contrarily, for the case of  $R_b = 1$ , the entire cross-section ( $D_{eq}$ ) can be assumed to be only subjected to uniform confinement pressure  $f_{l,f}^I = f_{l,eff} = f_{l,f}^{*FFSC}$ . Considering  $D_{eq}^I = D_{eq,c} = D_{eq}$  and  $D_{eq}^{II} = 0$ ,  $k_{h,eff} = 1$ . Accordingly, the following conditions should be considered to develop  $k_{h,eff}$  versus  $R_b$  relation:

- )a.  $k_{h,eff}$  increases with  $R_b$ .
- )b.  $k_{h,eff}$  approaches the value of 0.5 when  $R_b = 0$ .
- )c.  $k_{h,eff}$  approaches 1 when  $R_b = 1$ .

According to the aforementioned conditions, this relation can be estimated from the following second order parabolae:

$$k_{h,eff} \simeq 0.5(1 + 2R_b - R_b^2) \quad (21)$$

Ultimately,  $k_{h,eff}$  as an input parameter in Eq. (13) for the calculation of  $K_H$ , can be obtained using Eq. (21).

#### 4.3. Determination of $k_{eh}$

The reduction factor  $k_{eh}$ , which represents the ratio between  $\varepsilon_{h,eff}$  and  $\varepsilon_{h,m}$ , is determined in this section. Fig. 6a schematically illustrates the distribution of hoop strain on a quarter of a square cross-section and in

**Table 1**  
Test database of  $k_{eh}^{Exp}$  for the case of FFSC.

Reference	ID	b (mm)	$R_b$	$f_{co}$ (MPa)	$k_{eh}^{Exp}$	Reference	ID	b (mm)	$R_b$	$f_{co}$ (MPa)	$k_{eh}^{Exp}$
Ozbakkaloglu [6]	A10R15L3-1	150	0.20	77	0.77	Wang et al. [42]	S2H0L2C	204	0.20	26	0.46
	A10R15L3-2	150	0.20	77	0.86		S2H2L2C	204	0.20	33	0.60
	A10R30L3-1	150	0.40	77	1.00		S2H2L2C	204	0.20	33	0.52
	A10R30L3-2	150	0.40	77	0.61		S1H1L3M	305	0.20	32	0.42
	A10R15L5-1	150	0.20	77	0.27		S1H1L3M	305	0.20	32	0.55
	A10R30L5-1	150	0.20	77	0.56		VII-D2-M-M-1	250	0.20	47	0.78
Saleem et al. [12]	A10R30L5-2	150	0.40	77	0.61	VII-D2-M-M-1	250	0.20	47	0.80	
	SR13L1	150	0.17	24	0.66	VI-D4-M-M-1	250	0.20	39	0.71	
	SR13L2	150	0.17	24	0.34	VI-D4-M-M-1	250	0.20	39	0.80	
	SR26L1	150	0.35	24	0.89	VII-D3-M-M-2	250	0.20	47	0.61	
	SR26L2	150	0.35	24	0.74	VII-D3-M-M-2	250	0.20	47	0.63	
	SR26L3	150	0.35	24	0.59	VII-D3-M-M-2	250	0.20	47	0.63	
Suon et al. [8]	S13-3L	150	0.17	16	0.62	R150L1	150	0.25	25	0.57	
	S13-6L	150	0.17	16	0.61	P175L2	175	0.29	25	0.82	
	S13-9L	150	0.17	16	0.54	P350L4	350	0.23	22	0.64	
	S26-3L	150	0.35	16	0.72	R300L2	300	0.30	23	0.66	
	S26-6L	150	0.35	16	0.65	S-CR10-CLO	150	0.13	39	0.86	
	S26-9L	150	0.35	16	0.69	S-CR20-CLO	150	0.27	39	1.09	
Zhu et al. [39]	2sq1	150	0.33	32	0.63	C30N1r15	150	0.20	32	0.83	
	2sq1	150	0.33	32	0.59	C30N1r30	150	0.40	32	0.83	
	3sq1	150	0.33	32	0.60	C30N1r45	150	0.60	31	0.91	
	3sq2	150	0.33	32	0.52	C30N1r60	150	0.80	32	0.83	
	4sq1	300	0.33	23	0.73	C30N2r15	150	0.20	32	0.95	
	4sq2	300	0.33	23	0.71	C30N2r30	150	0.40	32	0.64	
Mostofinejad et al. [30]	S15	150	0.20	40	0.71	C30N2r45	150	0.60	31	0.80	
	S30	150	0.40	40	0.88	C30N2r60	150	0.80	32	0.94	
	S45	150	0.60	40	0.91	C50N1r15	150	0.20	54	0.67	
	S60	150	0.80	40	0.95	C50N1r30	150	0.40	52	0.82	
	S30	300	0.20	42	0.73	C50N1r45	150	0.60	53	0.89	
	S60	300	0.40	45	0.64	C50N1r60	150	0.80	53	1.05	
Shan et al. [10]	S90	300	0.60	45	0.88	C50N2r15	150	0.20	54	0.42	
	S120	300	0.80	45	0.93	C50N2r30	150	0.40	52	0.85	
	1S-1	150	0.40	34	0.95	C50N2r45	150	0.60	53	0.77	
	2S-1	150	0.40	34	0.67	C50N2r60	150	0.80	53	0.91	
	2S-1	150	0.40	34	0.73	S10r1	150	0.13	36	1.04	
	S-C2-0	279	0.14	17	0.78	S10r1-F	150	0.13	36	0.56	
Wang and Wu [40]	S-CS-0	279	0.14	17	0.62	S20r1	150	0.13	36	0.82	
	S-G6-0	279	0.14	17	0.38	S20r1-F	150	0.13	36	0.63	
	S-GS-0	279	0.14	17	0.49	S10r3	150	0.40	36	0.92	
	1S-1	150	0.40	34	0.95	S10r3-F	150	0.40	36	0.85	
	2S-1	150	0.40	34	0.67	S20r3	150	0.40	36	0.67	
	S-C2-0	279	0.14	17	0.78	S20r3-F	150	0.40	36	0.75	
Pantelides et al. [41]	S2H0L2C	204	0.20	26	0.28						
	S2H0L2C	204	0.20	26	0.28						

the quarter of the corresponding equivalent circular cross-section during axial compressive loading. Hoop strain at each corner zone ( $\epsilon_{h,c}$ ) was assumed to be less than  $\epsilon_{h,m}$  at the middle of the flat sides. Considering the effective hoop strain ( $\epsilon_{h,eff}$ ) equal to  $\epsilon_{h,c}$  based on Lee et al. [18] and Lin and Teng [24] for the case of FFSC, a homogeneous strain field in the perimeter of the equivalent circular column can be assured, in the compliance with hoop strain distribution in the circular section. Mostofinejad et al. [30] and Oliveira and Carrazedo [33] evidenced that the hoop strain distribution is strongly dependent on  $R_b$ . Table 1 presents a set of large test database of  $k_{eh}^{Exp} = \epsilon_{h,c}^{Exp} / \epsilon_{h,m}^{Exp}$  obtained from FFSC specimens, where  $\epsilon_{h,c}^{Exp}$  is assumed to represent  $\epsilon_{h,eff}$  in the column section perimeter ( $\epsilon_{h,eff}$  is an entity related to an equivalent column's cross-section, so it is not measurable experimentally). Accordingly, based on the best fit of experimental results, the following expression was derived as a linear function of  $R_b$  based on regression analysis:

$$k_{eh} = 0.5(1 + R_b) \tag{22}$$

In Eq. (22), for the cases of FFSC with sharp edges ( $R_b = 0$ ) and FFCC ( $R_b = 1$ ),  $k_{eh}$  would be equal to 0.5 and 1, respectively. Fig. 6b presents the predictive performance of Eq. (22). As can be seen, based on the mean value, standard deviation (SD) and mean absolute percentage error (MAPE, defined as  $MAPE = \frac{1}{N} \sum_{i=1}^N |1 - k_{eh}^{Ana} / k_{eh}^{Exp}|$  where  $N$  denotes the total test data number), the developed model is able to estimate the experimental counterparts with acceptable accuracy in the design

context. As a result, by taking into account the effect of non-uniform distribution of hoop strain along the perimeter of the section through the reduction factor  $k_{eh, J_{lf}^{FFSC}}$  can be obtained from Eq. (12) at a known value of  $\epsilon_{h,m}$ . Since the reduction factors of  $k_{h,f}$ ,  $k_{h,eff}$  and  $k_{eh}$ , as input parameters for  $K_H$  (Eq. (13)), were determined only as a function of  $R_b$ , a simplified  $K_H$  was developed by using regression analysis. Accordingly, the best-fit  $K_H$  was derived as a linear function of  $R_b$  with  $R^2 \simeq 1$  (Fig. 7):

$$K_H = R_b \geq 0.07 \tag{23}$$

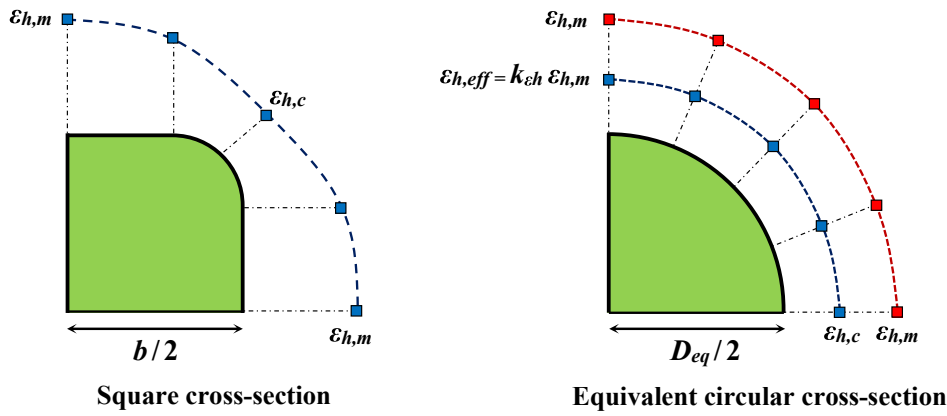
Accordingly, the horizontal confinement efficiency factor can be considered equal to the corner radius ratio ( $R_b$ ) with a lower bound of 0.07 for  $R_b \leq 0.07$ . In Fig. 7, the comparative evaluation of  $K_H$  obtained from Eq. (13) and that suggested by Mander et al. [28] ( $A_{eff}/A_g$ ) demonstrates that Eq. (13) leads to lower values of  $K_H$ . It is due to the consideration of  $k_{h,eff}$  and  $k_{eh}$  in the determination of the proposed  $K_H$ , besides the term  $k_{h,f}$ . Accordingly, taking into consideration that  $K_H$  suggested by Mander et al. [28] is based on OCCEE, which only formulates the term  $k_{h,f}$ , therefore a similar trend with  $k_{h,f}$  calculated by Eq. (17) is reasonably expected as highlighted in Fig. 7.

## 5. FRP confinement pressure of FFSC

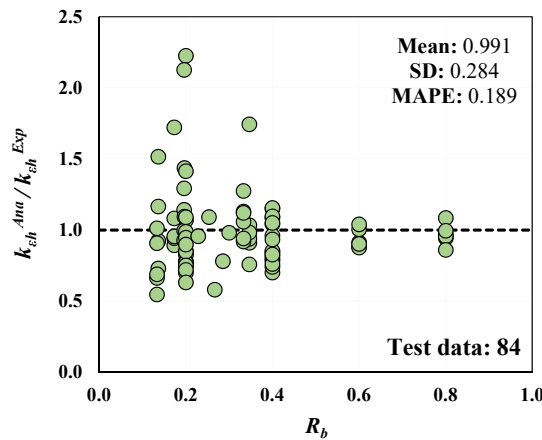
### 5.1. Influence of Non-homogenous concrete expansibility

By taking into consideration that radial strain ( $\epsilon_r(z)$ ) and hoop strain





a)



b)

Fig. 6. (a) Typical distribution of hoop strain field on the perimeter of a quarter of cross-section; (b) Predictive performance of  $k_{eh}$  model.

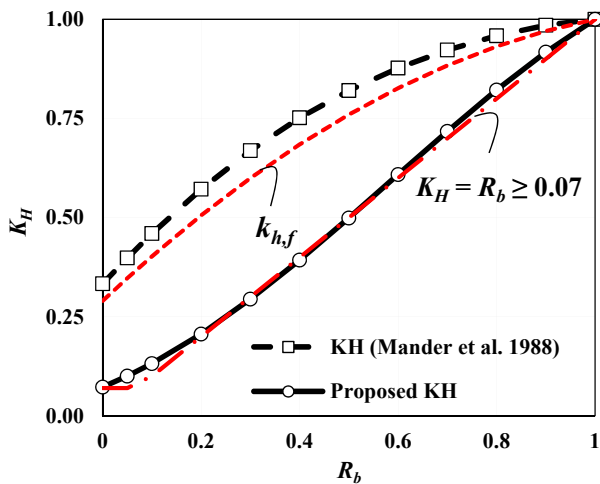


Fig. 7. Variation of  $K_H$  with  $R_b$ .

( $\epsilon_h(z)$ ) of a circular cross-section column are identical,  $f_{l,j}^{FFSC}$  presented in Eq. (12) can be only valid for the case of FFSC with a uniform concrete transverse expansibility along the column height ( $\epsilon_l(z) = \epsilon_{l,j}$ ) as illustrated in Fig. 8a. Here,  $\epsilon_{l,j}$  is the maximum radial strain due to concrete expansion, assumed to be located at the mid-height of the damage zone length ( $L_d$ );  $f_j^*$  is the corresponding generated FRP confining stress equal

to  $E_f \epsilon_{l,j}$  (Eq. (11) where  $\epsilon_{h,m} = \epsilon_{l,j}$ ). As can be seen in Fig. 8b and c, this laterally uniform concrete behavior leads to a uniform distribution of confining stress ( $f_f(z)$ ) and confinement pressure ( $f_{l,j}(z)$ ). However, the experimental evidence (Wei and Wu [45] and Fallahpour et al. [46]) demonstrated that during axial compressive loading, the concrete would non-homogeneously expand along the column height, since this transversal deformability profile strongly depends on the confinement stiffness. Accordingly, as presented in Fig. 8d, the ratio of  $\epsilon_l(z)$  and maximum concrete expansion ( $\epsilon_{l,j}$ ), denoted by  $k_\epsilon(z)$ , can be considered on the interval  $[k_\epsilon^{FFSC}, 1]$  where  $k_\epsilon^{FFSC}$  is the ratio of the minimum concrete expansion ( $\epsilon_{l,i}$ ) at the damage zone extremities and  $\epsilon_{l,j}$ , henceforward designated as ‘concrete expansion gradient’. Therefore, since  $f_f(z)$  is directly related with  $\epsilon_l(z)$ , non-uniform distributions for  $f_f(z)$  and, subsequently  $f_{l,j}(z)$ , are reasonably expected (Fig. 8e and f). Accordingly, in the present study, by assuming a second order parabola function for  $k_\epsilon(z)$  by supposing  $k_\epsilon(0) = k_\epsilon(L_d) = k_\epsilon^{FFSC}$ ,  $k_\epsilon(L_d/2) = 1$  and  $dk_\epsilon(L_d/2)/dz = 0$ , the ratio of average concrete expansion within  $L_d$  and  $\epsilon_{l,j}$  ( $k_{ff}^{FFSC}$ ) can be determined by taking the integration of  $k_\epsilon(z)$  function with respect to  $z$ -axis on the interval  $[0, L_d]$  ( $k_{ff}^{FFSC} = \int_{z=0}^{z=L_d} k_\epsilon(z) dz / L_d$ ). Hence, by solving this integration,  $k_{ff}^{FFSC}$  is derived as a function of concrete expansion gradient  $k_\epsilon^{FFSC}$ , regardless of  $L_d$  as:

$$k_{ff}^{FFSC} = \frac{1}{3} + \frac{2}{3} k_\epsilon^{FFSC} \quad (24)$$

By considering  $\epsilon_h(z) = \epsilon_l(z)$ , which is as  $\epsilon_{h,m} = \epsilon_{l,j}$  at  $z = L_d/2$ ,  $f_f(z)$  can be expressed by  $E_f \epsilon_l(z)$ , as revealed in Fig. 8e. By taking into

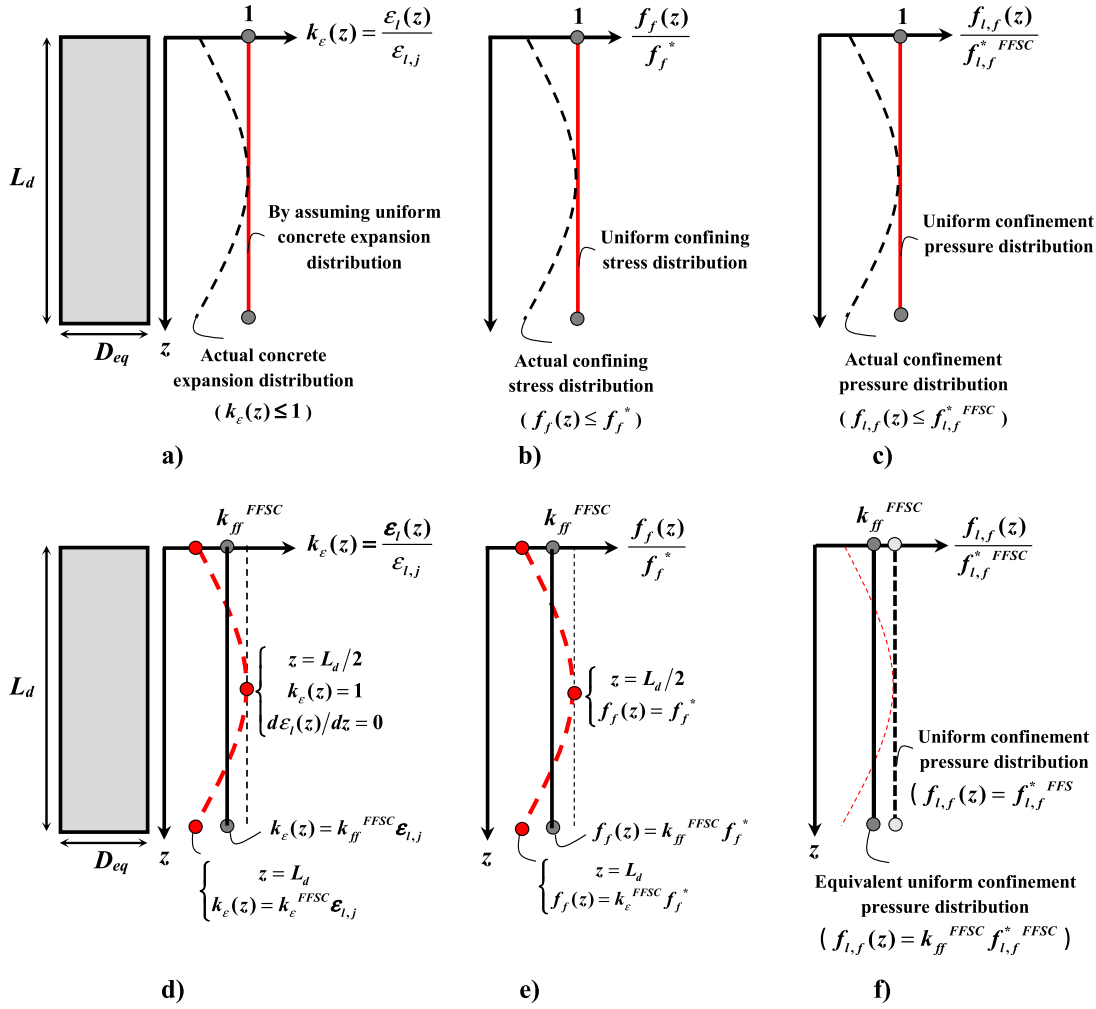


**Fig. 8.** Schematic distributions of concrete expansion gradient ( $k_e(z)$ ), normalized confining stress ( $f_f(z)/f_f^*$ ) and normalized confinement pressure ( $f_{l,f}(z)/f_{l,f}^{FFSC}$ ).

consideration that the equivalent homogenous concrete expansibility can be represented by  $k_{ff}^{FFSC} \epsilon_{i,j}$ , the generated average FRP confining stress, where the concrete is assumed to be evenly subjected to confining stress, would be  $k_{ff}^{FFSC} E_f \epsilon_{i,j}$ . Supposing  $f_f^* = E_f \epsilon_{i,j}$  based on Eq. (18),  $f_f(z)$  is obtained with a constant function as:

$$f_f(z) = k_{ff}^{FFSC} E_f \epsilon_{i,j} = k_{ff}^{FFSC} f_f^* \quad (25)$$

Since  $f_{l,f}(z)$  is directly related with  $f_f(z)$ , the ratio of equivalent homogenous confinement pressure ( $f_{l,f}^{FFSC}$ ) and  $f_{l,f}^{FFSC}$  can be expressed as (Fig. 8f):

$$\frac{f_{l,f}^{FFSC}}{f_{l,f}^{FFSC}} = \frac{k_{ff}^{FFSC} f_f^*}{f_f^*} \rightarrow f_{l,f}^{FFSC} = k_{ff}^{FFSC} f_{l,f}^{FFSC} \quad (26)$$

Putting Eq. (12) into Eq. (26) gives:

$$f_{l,f}^{FFSC} = k_{ff}^{FFSC} \times 2K_H \frac{n_f I_f}{D_{eq}} f_f^* = 2k_{ff}^{FFSC} K_H \frac{n_f I_f}{D_{eq}} E_f \epsilon_{i,j} \quad (27)$$

Thus, to calculate  $f_{l,f}^{FFSC}$ , the reduction factor  $k_{ff}^{FFSC}$ , which is dependent on the concrete expansion gradient ( $k_e^{FFSC}$ ) based on Eq. (24), needs to be addressed as an input parameter.

### 5.2. Determination of concrete expansion gradient ( $k_e^{FFSC}$ )

According to Wei and Wu [45] and Fallahpour et al. [46],  $k_e^{FFSC}$  representing the ratio of  $\epsilon_{l,i}$  at the damage zone extremities and  $\epsilon_{i,j}$  is

strongly dependent on confinement stiffness. Fallahpour et al. [46] revealed that homogenous axial and dilation behavior of the concrete along the column height can be only expected for the case of FFCC with high confinement stiffness. In fact, above a certain FRP confinement stiffness, the gradient of concrete transversal expansibility along the column height is almost null, due to the strong restrictions imposed by the confinement system to the concrete. On the other hand, for FFCC with low confinement stiffness, since the confinement system is not stiff enough to efficiently homogenize the evolution of damage due to cracking propagation, which subsequently induces to local strain gradients, non-homogenous concrete expansion in the vertical direction is highly expected ([45–47]). In the present study, the confinement stiffness index ( $I_f$ ) proposed by Teng et al. [17], originally developed for FFCC, was adopted. For the case of FFSC, by reflecting the influence of horizontal arching action on the confinement stiffness through  $K_H$ ,  $I_f$  is introduced as:

$$I_f = \frac{f_{l,f}^{FFSC} / (k_{ff}^{FFSC} \epsilon_{i,j})}{f_{c0} / \epsilon_{c0}} = 2K_H \frac{n_f I_f E_f \epsilon_{c0}}{D_{eq} f_{c0}} \quad (28)$$

in which

$$\epsilon_{c0} = 0.0015 + \frac{f_{c0}}{70000} \quad (\text{in MPa}) \quad (29)$$

where  $f_{c0}$  is the axial compressive strength of unconfined concrete;  $\epsilon_{c0}$  is the axial strain corresponding to  $f_{c0}$ . Fig. 9 schematically demonstrates the distribution of concrete expansion gradient  $k_e(z)$  as a function

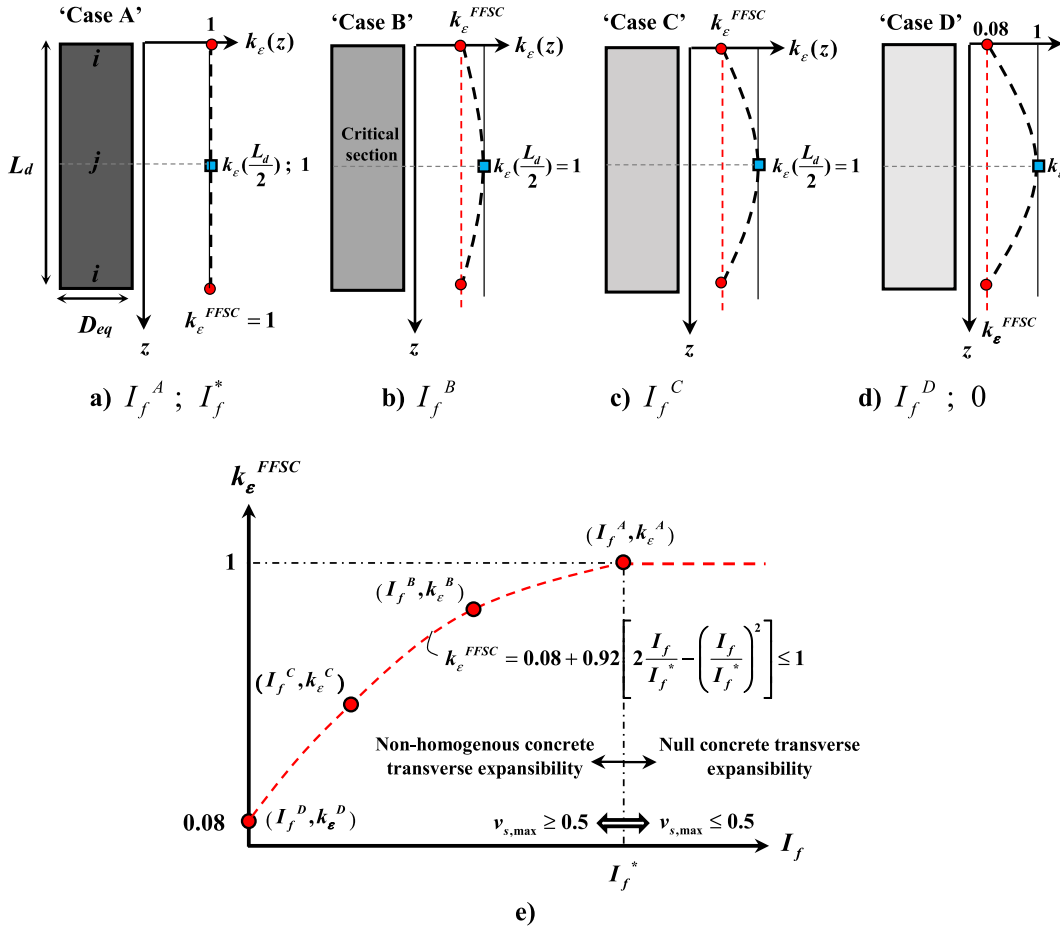


**Fig. 9.** (a-d) Schematic distribution of concrete expansion gradient  $k_e(z)$  as a function of  $I_f$ ; e) Relation of concrete expansion gradient  $k_e^{FFSC}$  and  $I_f$ ; **Note:**  $I_f^A \approx I_f^* < I_f^B < I_f^C < I_f^D \approx 0$ .

of  $I_f$ . As can be seen, from Case A (high level of  $I_f$ ) to Case D ( $I_f \approx 0$ ),  $k_e^{FFSC}$  decreases from 1 to 0.08, on the interval  $[0.08, 1]$ , being this last case representative of a dilation behavior of unconfined concrete. In this study, it was assumed that for  $I_f \geq I_f^*$ , the level of confinement stiffness is proficiently high to assure an almost homogenous concrete dilation response along the damage zone, leading to  $k_e^{FFSC} = 1$ . Under the same  $k_e(z = L_d/2) = 1$ , for  $I_f < I_f^*$ , confinement stiffness can be considered unable to fully homogenize the evolution of damage, leading to  $0.08 \leq k_e^{FFSC} < 1$  as demonstrated in Fig. 9. Owing to the lack of adequate experimental evidence for obtaining  $I_f^*$ , in this study, this confinement stiffness limit was determined based on the influence of confinement stiffness in terms of concrete volumetric strain response. Note that volumetric strain ( $\varepsilon_v$ ) at a location along the column height is defined as  $\varepsilon_v = \varepsilon_c - 2\varepsilon_l(z)$ , whose positive and negative values ( $\varepsilon_v > 0$  and  $\varepsilon_v < 0$ ), in the adopted convention of signals for strains, represent volumetric contraction and expansion, respectively. For the case of high level of  $I_f$  ( $I_f \geq I_f^*$  leading to  $k_e^{FFSC} = 1$ ,  $\varepsilon_l(z) = \varepsilon_{lj}$  and  $\varepsilon_v = \varepsilon_c - 2\varepsilon_{lj}$ ), the concrete can be assumed to experience contraction with reduction of its volume during entire axial loading history (Mirmiran and Shahawy [48] and Xiao and Wu [49]). Accordingly, whereas a significant compaction (compressive strain) would occur vertically, the gradient of concrete transversal expansibility along the column height is almost null due to the strong restrictions imposed by FRP confinement. Therefore, considering the secant Poisson's ratio ( $\nu_s = \varepsilon_{lj}/\varepsilon_c$ ) is equal to 0.5 when  $\varepsilon_v = 0$ , in the present study,  $I_f^*$  is introduced as a confinement stiffness index by which the maximum secant Poisson's ratio ( $\nu_{s,max}$ ) experienced by the concrete during axial loading does not exceed  $\nu_{s,max} = 0.5$ . Some

equations have been proposed by the analytical studies [35,48–53] to calculate  $\nu_{s,max}$  as a main function of confinement stiffness. By following Shayanfar et al. [35]'s recommendation,  $I_f$  can be expressed as a function of  $\nu_{s,max}$ :

$$I_f = \left( \frac{0.155}{(1.23 - 0.003f_{c0})\nu_{s,max}} \right)^2 \quad (30)$$

Accordingly, when  $\nu_{s,max} = 0.5$  as the input value, the corresponding  $I_f$  actually represents  $I_f^*$ . For the sake of simplicity, based on Eq. (30) with  $\nu_{s,max} = 0.5$ ,  $I_f^*$  was developed as ( $R^2 \approx 0.98$ ):

$$I_f^* = 0.06 + 0.0005f_{c0} \text{ (in MPa)} \quad (31)$$

Hence, as shown in Fig. 9e, for  $I_f < I_f^*$ , a non-uniform concrete lateral expansion with  $\nu_{s,max} > 0.5$  would be expected, while for  $I_f > I_f^*$ , the gradient of concrete expansibility along the column height is assumed as almost null with  $\nu_{s,max} < 0.5$ . By considering  $k_e^{FFSC}$  is on the interval  $[0.08, 1]$ , and assuming  $k_e^{FFSC}$  exclusively dependent on  $I_f$  according to a second order parabola function in which  $dk_e^{FFSC}/dI_f = 0$  at  $I_f = I_f^*$ , it results:

$$k_e^{FFSC} = 0.08 + 0.92 \left[ 2 \frac{I_f}{I_f^*} - \left( \frac{I_f}{I_f^*} \right)^2 \right] \leq 1 \text{ for } I_f \leq I_f^* \quad (32a)$$

$$k_e^{FFSC} = 1 \text{ for } I_f \geq I_f^* \quad (32b)$$

After obtaining  $k_e^{FFSC}$  through Eq. (32),  $k_{ff}^{FFSC}$  is determined by using Eq. (24). Thus,  $f_{if}^{FFSC}$  (the equivalent homogenous confinement pressure)

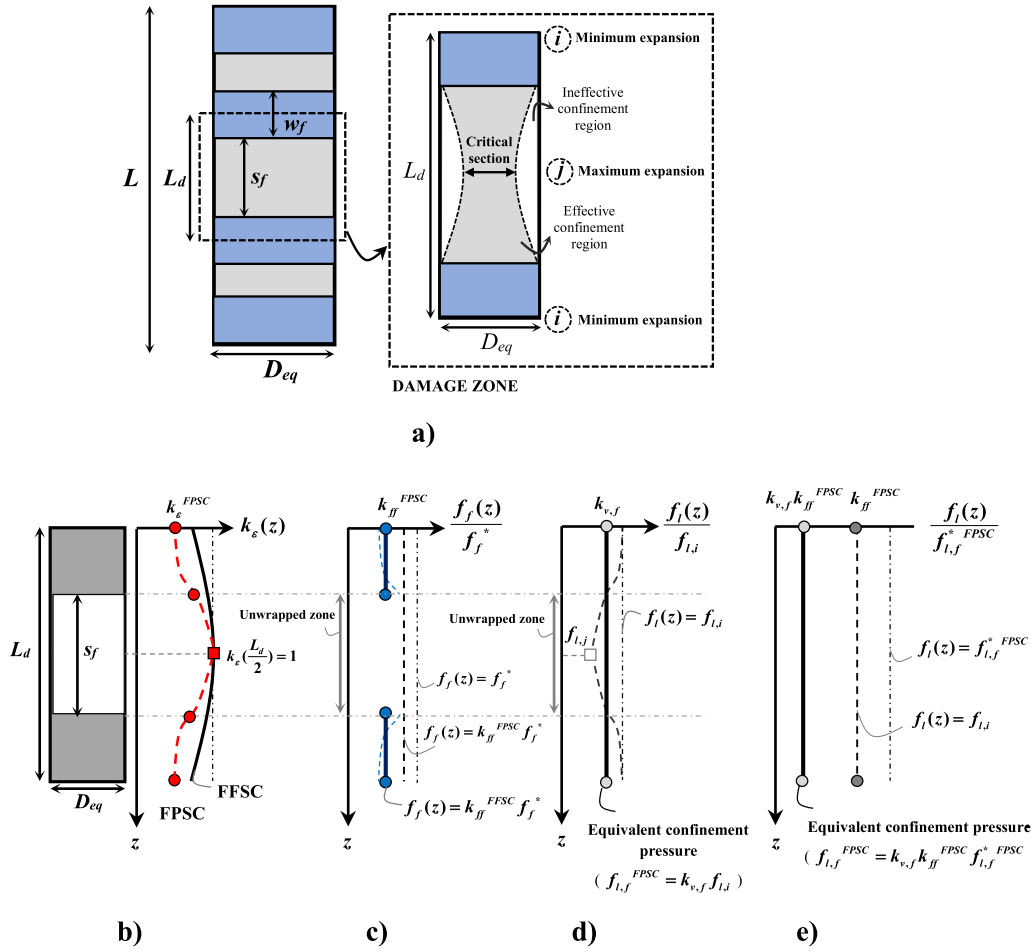


Fig. 10. (a) Partial confinement configuration; b) Concrete lateral expansion distribution; c) FRP confining stress distribution; d-e) Confinement pressure distribution.

can be calculated by Eq. (27), reflecting the effect of non-homogenous distribution of concrete expansion along the column height through  $k_{ff}^{FPSC}$ .

### 6. FRP confinement pressure of FPSC

The confinement characteristics of a concrete column of square cross-section with a FRP partial confinement configuration, FPSC, under axial compressive loading will be determined by extending the previous formulation of the FFSC in order to have a unified approach. Fig. 10a demonstrates the confinement configuration in the case of FPSC, where  $w_f$  and  $s_f$  are the width and the distance between two consecutive FRP strips. In Fig. 10b represents the typical distribution of concrete transverse expansibility of FPSC within the damage zone ( $L_d$ ). As expected, for the case of FPSC, the concrete expansibility distribution would be more predominantly non-homogenous compared to FFSC, with  $k_e(z=0) = k_e(z=L_d) = k_e^{FPSC}$  and  $k_e(z=L_d/2) = 1$ . Considering  $k_{ff}^{FPSC}$  is the ratio of average concrete expansion within the wrapped zone and at  $z = L_d/2$ ,  $\epsilon_{l,j}$ , the corresponding generated confining stress would be as  $f_f(z) = E_f k_{ff}^{FPSC} \epsilon_{l,j}$ , which can be expressed as  $f_f(z) = k_{ff}^{FPSC} f_f^*$  based on Eq. (25), as shown in Fig. 10c. It should be noted that for the case of full confinement system (supposing as a special case of FPSC with  $R_f = s_f/D_{eq} = 0$ ), to establish a unified framework for FFSC and FPSC,  $k_{ff}^{FPSC}$  should be equal to  $k_{ff}^{FFSC}$  when  $R_f = 0$ . Due to vertical arching action, confinement pressure function  $f_l(z)$  generated by  $f_f(z)$  decreases from  $f_{l,i}$  (the maximum confinement pressure at the Point  $i$ ) to  $f_{l,j}$  (the minimum

confinement pressure at the Point  $j$  where the effective confinement area has the lowest diameter, leading to the weakest confinement restriction), Fig. 10a. Accordingly, as shown in Fig. 10d, to obtain an equivalent confinement pressure ( $f_{l,f}^{FPSC}$ ) homogeneously acting on the entire column height, a reduction factor  $k_{v,f}$  is introduced, which can be determined by integrating  $f_l(z)$  function with respect to  $z$ -axis on the interval  $[0, L_d]$  ( $k_{v,f} = \int_{z=0}^{z=L_d} f_l(z) dz / L_d$ ), leading to  $f_{l,f}^{FPSC} = k_{v,f} f_{l,i}$ .

On the other hand, by assuming a constant concrete expansibility ( $k_{ff}^{FPSC} = 1$ ) and neglecting the vertical arching action mechanism ( $k_{v,f} = 1$ ), the confinement pressure of FPSC,  $f_{l,f}^{FPSC}$ , can be determined based on the equilibrium of confinement forces:

$$f_{l,f}^{FPSC} = 2K_H \frac{n_f t_f w_f}{(s_f + w_f) D_{eq}} f_f^* \quad (33)$$

In order to address the influence of concrete expansibility, based on Eq. (26), considering  $f_f(z) = k_{ff}^{FPSC} f_f^*$ , the ratio of  $f_{l,f}^{FPSC}$  and  $f_{l,i}^{FPSC}$  can be written as (Fig. 10e):

$$\frac{f_{l,i}}{f_{l,f}^{FPSC}} = \frac{k_{ff}^{FPSC} f_f^*}{f_f^*} \rightarrow f_{l,i} = k_{ff}^{FPSC} f_{l,f}^{FPSC} \quad (34)$$

Considering  $f_{l,f}^{FPSC} = k_{v,f} f_{l,i}$ , and replacing Eq. (33) into Eq. (34) yields:

$$f_{l,f}^{FPSC} = k_{v,f} f_{l,i} = 2k_{v,f} k_{ff}^{FPSC} K_H \frac{n_f t_f w_f}{(s_f + w_f) D_{eq}} E_f \epsilon_{l,j} \quad (35)$$

Assuming that  $k_{ff}^{FPSC}$  is on the interval  $[0.08, k_{ff}^{FFSC}]$  where  $k_{ff}^{FFSC} \approx 0.08$

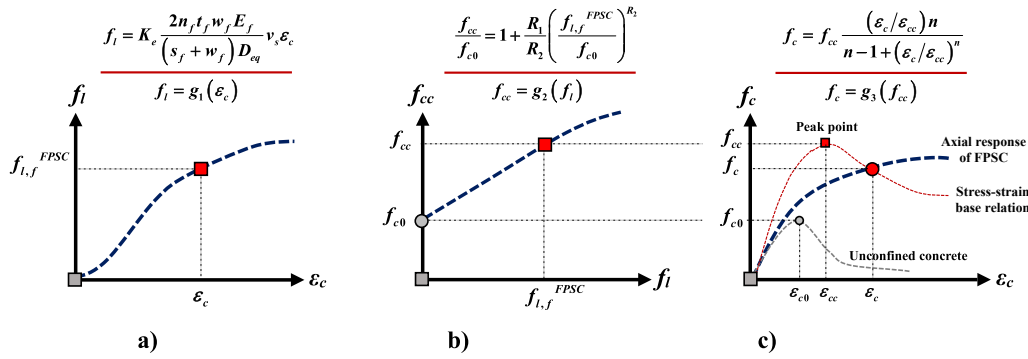


Fig. 11. Determination of axial response of FRP confined concrete: a) Confinement pressure versus axial strain; b) Peak axial stress versus confinement pressure; c) Axial stress versus axial strain.

for  $s_f \geq L_{d0}$  (representing that confinement pressure imposed by FRP strips mainly acts on the concrete out of the damage zone based on the experimental observations by Barros and Ferreira [4], Zeng et al. [3] and Wang et al. [54]), and  $k_{ff}^{FPSC} = k_{ff}^{FPSC}$  at  $s_f = 0$  (supposing as a special case of FPSC with  $R_f = s_f/D_{eq} = 0$ , to establish a unified framework for FPSC and FPSC). Accordingly,  $k_{ff}^{FPSC}$  as a linear function of  $s_f/L_{d0}$  can be determined by:

$$k_{ff}^{FPSC} = k_{ff}^{FPSC} - (k_{ff}^{FPSC} - 0.08) \frac{s_f}{L_{d0}} \geq 0.08 \quad (36)$$

where  $L_{d0}$  can be calculated as recommended by Wu and Wei [47], which is based on the approach of localized compressive fracture length developed by Lertsrisakulrat et al. [55], as follows:

$$0.57 \leq \frac{L_{d0}}{D_{Ler} \psi_f} = 1.71 - 3.53 \times 10^{-5} D_{Ler}^2 \leq 1.36 \quad (37)$$

$$D_{Ler} = \sqrt{A_g} = b \sqrt{1 - 0.215 R_b^2} \quad (38)$$

$$\psi_f = \frac{6.3}{\sqrt{f_{c0}}} \leq 1 \quad (39)$$

where  $A_g$  is the total area of the section. To address the influence of vertical arching action, in this study, the Shayanfar et al. [35]’ recommendation to calculate  $k_{v,f}$  originally developed for FPCC, was adopted for the equivalent circular section column of FPSC, as follows:

$$k_{v,f} = \frac{w_f + s_f (1 - R_f + 0.43 R_f^2 - 0.07 R_f^3)}{w_f + s_f} \leq 1 \quad (40)$$

in which

$$R_f = \frac{s_f}{D_{eq}} \quad (41)$$

As a result, based on Eq. (35), the equivalent confinement pressure ( $f_{l,f}^{FPSC}$ ) can be rearranged as follows:

$$f_{l,f}^{FPSC} = 2K_e \frac{n_f t_f w_f}{(s_f + w_f) D_{eq}} E_f \epsilon_{i,j} \quad (42)$$

in which

$$K_V = k_{v,f} k_{ff}^{FPSC} \quad (43)$$

$$K_e = K_H K_V \quad (44)$$

where  $K_e$  (Eq. (44)) can be regarded as the ‘confinement efficiency factor’ consisting of two components as  $K_H$  (Eq. (23)) and  $K_V$  (Eq. (43)), reflecting the influence of non-uniform concrete expansion and arching action in the equivalent confinement pressure  $f_{l,f}^{FPSC}$ .

## 7. Proposed axial Stress–strain model

In this section, the determination of the axial stress versus axial strain curve ( $f_c$  vs  $\epsilon_c$  curve) of FRP confined concrete subjected to axial compressive loading will be addressed based on active confinement approach (i.e. [15–24]). In this approach, at a certain concrete axial strain  $\epsilon_c$ , the corresponding confinement pressure ( $f_l$ ) is derived based on a dilation model, which can be expressed as a function of  $\epsilon_c$  leading to  $f_l = g_1(\epsilon_c)$  (Fig. 11a). Moreover, the axial response of FRP confined concrete is derived based on an axial stress–strain base relation model (Fig. 11c), developed for AFCC, whose characteristics are strongly dependent of its peak axial stress point ( $f_{cc}$ ). Furthermore, since  $f_{cc}$  is essentially dependent on the level of confinement pressure ( $f_l$ ), an axial strength model ( $f_{cc} = g_2(f_l)$ ) requires to be established (Fig. 11b). Therefore, the corresponding axial stress ( $f_c$ ) can be obtained by following the axial stress–strain base relation model as a function of  $f_{cc}$  which is presented as  $f_c = g_3(f_{cc})$ . In this study, for the case of FPSC, the axial stress–strain base framework (function  $g_3$ ) recommended by Popovics [25] (originally suggested for AFCC) was adopted as (Fig. 11c):

$$f_c = g_3(f_{cc}) = f_{cc} \frac{(\epsilon_c/\epsilon_{cc})^n}{n-1 + (\epsilon_c/\epsilon_{cc})^n} \quad (45)$$

in which

$$\frac{\epsilon_{cc}}{\epsilon_{c0}} = 1 + 5 \left( \frac{f_{cc}}{f_{c0}} - 1 \right) \quad (46)$$

$$n = \frac{E_c}{E_c - f_{cc}/\epsilon_{cc}} \quad (47)$$

where  $\epsilon_{cc}$  is the axial strain corresponding to  $f_{cc}$  which was determined by Mander et al. [28]’s recommendation;  $n$  is the concrete brittleness suggested by Carreira and Chu [56];  $E_c$  is the modulus elasticity of concrete, which can be calculated as  $E_c = 4730 \sqrt{f_{c0}}$  (ACI-318-08 [57]).

Several axial strength models (i.e. [15–17,20,22]) have been proposed to calculate  $f_{cc}$  and  $f_l$  relation ( $f_{cc} = g_2(f_l)$ ). Conventionally, for the sake of simplicity, at a certain  $\epsilon_c$  leading to a specific  $f_l$  ( $f_l = g_1(\epsilon_c)$ ), the corresponding  $f_{cc}$  is assumed to be identical to that of actively-confined concrete (AFCC) where concrete is subjected to constant  $f_l$  during the entire axial loading. Therefore, for the establishment of function  $g_2$ , those models suggested/calibrated for AFCC can be also followed for the case of FRP confined concrete. However, based on studies conducted by Lim and Ozbakkaloglu [20], Yang and Feng [22] and Lin et al. [23], this assumption would lead to overestimations in terms of confinement-induced improvements offered by FRP confined concrete. It is due to their different confinement pressure paths-based axial strain ( $f_l$  versus  $\epsilon_c$  relation), where FRP confined concrete experiences a non-constant confinement pressure during the entire axial loading (Fig. 11a) contrary to AFCC with a constant function. In the present study, by taking

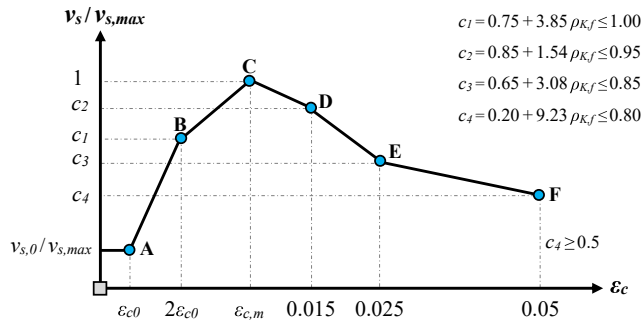


Fig 12. Relation between  $\alpha_{ec} = v_s/v_{s,max}$  and  $\epsilon_c$  (redrawn from Shayanfar et al. [35]).

into account the confinement path effect, a new axial strength model was proposed by introducing the function  $g_2$ , whose parameters were derived from global axial stress–strain curve of test specimens of FFCC, FFSC, FPCC and FPSC (with the confinement path effect) rather than AFCC, was proposed based on regression analysis technique, as

$$\frac{f_{cc}}{f_{c0}} = 1 + \frac{R_1}{R_2} \left( \frac{f_{lf}^{FPSC}}{f_{c0}} \right)^{R_2} = 1 + \frac{R_1}{R_2} \left( \rho_{K,f} \frac{v_s \epsilon_c}{\epsilon_{c0}} \right)^{R_2} \quad (48)$$

where  $R_1$  and  $R_2$  are the calibration terms, which need to be addressed based on the global axial stress–strain of the experimental results. In Eq. (48),  $v_s$  is the secant Poisson ratio corresponding to  $\epsilon_c$  ( $v_s = \epsilon_{lj}/\epsilon_c$ );  $\rho_{K,f}$  is the confinement stiffness index, which can be expressed as:

$$\rho_{K,f} = \frac{f_{lf}^{FPSC} / \epsilon_{lj}}{f_{c0} / \epsilon_{c0}} = 2K_e \frac{n_f t_f w_f E_f \epsilon_{c0}}{(s_f + w_f) D_{eq} f_{c0}} \quad (49)$$

Due to the unified character of the developed confinement model, Eq. (49) can be assumed valid for all cases of FFCC, FPCC, FFSC and FPSC. In the present study, to calculate  $v_s$  corresponding to  $\epsilon_c$ , Shayanfar et al. [35] dilation model, which has a unified character for both full and partial confinement systems as its unique advantage, was followed with a slight rearrangement:

$$v_s = \alpha_{ec} v_{s,max} \quad (50)$$

where  $\alpha_{ec}$  represents the ratio of  $v_s$  corresponding to  $\epsilon_c$  and  $v_{s,max}$ , being this relationship dependent on  $\rho_{K,f}$ , as shown in Fig. 12. Here,  $v_{s,0}$  is the initial Poisson's ratio of unconfined concrete that can be calculated by (Candappa et al. [58]):

$$v_{s,0} = 8 \times 10^{-6} f_{c0}^2 + 2 \times 10^{-4} f_{c0} + 0.138 \quad (51)$$

Furthermore,  $v_{s,max}$  is the maximum secant Poisson ratio corresponding to the axial strain of  $\epsilon_{c,m}$ , which was empirically suggested by Shayanfar et al. [35] as (with a slight modification by introducing the concept of equivalent diameter):

$$v_{s,max} = \frac{0.256}{\left( 1 + \frac{L_{eq}}{D_{eq}} \right) \sqrt{\rho_{K,f}}} \quad (52)$$

$$\epsilon_{c,m} = 0.0085 - 0.05 \rho_{K,f} \quad (53)$$

It is noteworthy that according to the adopted dilation model, as demonstrated in Fig. 12, by increasing  $\epsilon_c$  up to  $\epsilon_{c0}$ , initial concrete expansion is considered equal to that of unconfined concrete ( $v_s = v_{s,0}$ ). Afterward, for  $\epsilon_{c0} \leq \epsilon_c \leq 2\epsilon_{c0}$ , owing to the Poisson's ratio effect,  $v_s$  would increase with a faster rate, leading to the formation of splitting cracks and a considerable lateral stiffness degradation. Since the significant activation of FRP confining pressure is also expected in this stage, the magnitude of change of  $v_s$  is a function of confinement stiffness ( $\rho_{K,f}$ ) so

that by increasing  $\rho_{K,f}$ , the width and development of splitting cracks are restricted. Beyond this stage, by the degeneration of micro- into meso- and macro-cracks,  $v_s$  experiences its maximum value ( $v_{s,max}$ ) at  $\epsilon_{c,m}$ , which is then followed by a reduction in concrete tendency to dilate as a function of  $\rho_{K,f}$ , even though the concrete lateral strain becomes increasingly larger. More information regarding the dilation mechanism of FRP confined concrete can be found in [35,53,59]. Therefore, by using this dilation model coupled with the proposed axial strength model, at every level of  $\epsilon_c$ , the corresponding  $v_s$  as an input parameter in Eq. (48) can be calculated.

In order to determine the calibration terms of  $R_1$  and  $R_2$  in Eq. (48), the following equations were proposed using a back analysis, based on the best fitting with the experimental results of FRP confined concrete specimens collected in the test database (Appendix A):

$$R_1 = \frac{23.9 \rho_{K,f}^{0.67}}{\lambda_{fc} \lambda_{Rb} \lambda_{Rf}} \leq 4.25 \quad (54)$$

$$R_2 = 1.85 \rho_{K,f}^{0.26} \geq 0.3 \quad (55)$$

in which

$$\lambda_{fc} = 0.75 + 0.008 f_{c0} \quad (56)$$

$$\lambda_{Rb} = 1.5(1 - 1.1 R_b) \geq 1 \quad (57)$$

$$\lambda_{Rf} = 1 + 0.5 R_f \quad (58)$$

where  $\lambda_{fc}$ ,  $\lambda_{Rb}$  and  $\lambda_{Rf}$  are the calibration factors of  $R_1$ , reflecting the influence of  $f_{c0}$ ,  $R_b$  and  $R_f$ , respectively. It is well-established that compared to normal-strength concrete, high-strength concrete would experience a longer lag between the development of axial strain and the generation of confining strain and stress due to the higher stiffness and smaller transversal deformation [60,61]. Accordingly, during axial compressive loading, at a certain level of  $f_{lf}^{FPSC}/f_{c0}$ , FRP confinement-induced improvements (as stress-path dependent) in high-strength concrete would be not so pronounced than those in normal-strength concrete. In this study, this phenomenon was addressed by using the calibration factors of  $\lambda_{fc}$  in the evaluation of  $f_{cc}$ .

In the works of Ho et al. [60] and Lai et al. [61], a confinement path effect ( $\Delta$ ) is introduced as the difference between the peak axial strength ( $f_{cc}$ ) of passively FRP confined concrete and that obtained from an axial strength model suggested for the case of actively-confined concrete ( $f_{cc}^{Active}$ ), i.e.,  $\Delta = f_{cc} - f_{cc}^{Active}$ . Accordingly, to evaluate the confinement path effect during axial loading, an axial strength model of actively-confined concrete can be adopted to calculate  $f_{cc}^{Active}$  (i.e. as suggested by Lim and Ozbakkaloglu [20]). Then, at every level of  $f_{lf}^{FPSC}/f_{c0}$ ,  $\Delta$  can be determined quantitatively based on the corresponding  $f_{cc}$  (Eq. (48)). A comprehensive review of confinement path effect ( $\Delta$ ) can be found in Lim and Ozbakkaloglu [20], Ho et al. [60] and Lai et al. [61].

It should be also noted that since the experimental values of  $R_1$  and  $R_2$  (as input parameter for  $f_{cc}$ ) cannot be directly derived from experimental axial responses ( $f_c$  vs  $\epsilon_c$ ), in this study, an iterative solution procedure based on regression analysis technique was adopted to derive the experimental counterparts of these calibration terms. Accordingly, first, the developed confinement model was applied to 418 test specimens of FFCC, FPCC, FFSC and FFPC (Appendix A), then the values of  $R_1/R_2$  and  $R_2$  were determined based on the best-fit of the model with the experimental global axial stress–strain curves. Subsequently, the best-fit of relation of  $R_1$  and  $R_2$  with  $\rho_{K,f}$  was obtained by using regression analyses. At the second stage, this procedure was repeated by implementing the confinement model on the test specimens but by using the  $R_2$  achieved from the previous stage, as presented in Eq. (55). Then, the experimental values of  $R_1$  was re-derived based on the best-fit of the model with the experimental counterparts in terms of global axial stress–strain curves. Finally, based on regression analysis, the relation of

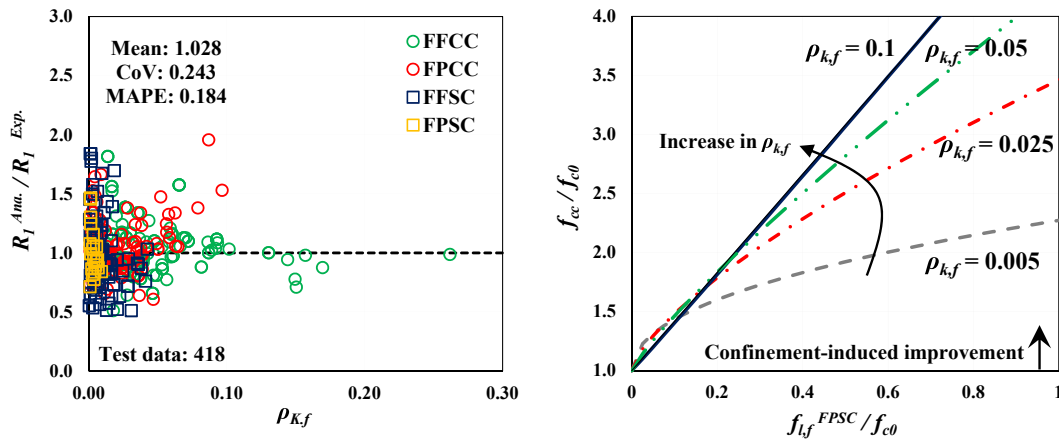


Fig. 13. Assessment of a) the correlation of Eq. (54); b) the variation of Eq. (48) with different  $\rho_{k,f}$ .

$R_1$  with  $\rho_{k,f}$  was developed by taking into account the influence of  $f_{c0}$ ,  $R_b$  and  $R_f$ , as presented in Eq. (54). Note that due to the framework of Eq. (48) in the representation of  $f_{cc}/f_{c0}$  and  $f_{l,f}^{FPSC}/f_{c0}$  relationship, the first stage of the procedure was repeated several times until the best-fit relations of the derived  $R_1/R_2$  and  $R_2$  with  $\rho_{k,f}$  were nearly converged. In the case of the typical axial strength model framework as  $f_{cc}/f_{c0} = 1 + R_1 (f_{l,f}^{FPSC}/f_{c0})$  with  $R_2 = 1$ , no iterative solution procedure is needed. Nonetheless, the preliminary comparative assessment of the proposed framework of Eq. (48) with the framework where  $R_2 = 1$  is considered, revealed a better predictive performance of Eq. (48) in terms of FRP confinement-induced improvements, which was derived based on the described iterative solution procedure. To assess the correlation of Eq. (54), the results provided by the developed equation determining  $R_1$  are compared in Fig. 13a with the ones extracted from experimental results. As shown, based on the mean value, coefficient of variation (COV) and MAPE (defined as  $MAPE = \frac{1}{N} \sum_{i=1}^N |1 - R_1^{Ana}/R_1^{Exp}|$  where  $N$  denotes the total test data number), the proposed expression has an acceptable predictive performance for estimating the  $R_1^{Exp}$  obtained from experimental studies of FFCC, FPCC, FFSC and FPSC.

Fig. 13b demonstrates the variation of FRP confinement-induced improvements in terms of  $f_{cc}/f_{c0}$  versus  $f_{l,f}^{FPSC}/f_{c0}$  relation of FRP confined concrete with  $R_b = 0.3$  and  $R_f = 0.3$ , obtained from Eq. (48) by assuming  $\lambda_{fc} = 1$ ,  $\lambda_{Rb} = 1.005$  and  $\lambda_{Rf} = 1.15$ , based on the various ranges of  $\rho_{k,f}$  as 0.005 (2.15), 0.025, 0.05 and 0.1. As can be seen, the confinement-induced improvements are mainly dependent on  $\rho_{k,f}$ , reflecting the confinement path effect. By increasing  $\rho_{k,f}$ , at the certain  $f_{l,f}^{FPSC}/f_{c0}$ ,  $f_{cc}/f_{c0}$  representing the effectiveness of confinement pressure in axial strength improvement is considerably enhanced, particularly for higher  $\rho_{k,f}$ .

The test database (Appendix A) consists of a total of 418 FRP confined concrete columns tested under axial compression collected from the literature, in which 155 specimens are as FRP fully confined circular columns (FFCC), 136 specimens are as FRP partially confined circular columns (FPCC), 105 specimens are as FRP fully confined square columns (FFSC), and 22 specimens are as FRP partially confined square columns (FPSC). The assumed selection criteria for choosing the experimental data available in the assembled database are as follows: 1) Test specimens under axial concentric loading were included; 2) Test specimens with circular and square cross-section were included; 3) Test specimens confined by unidirectional fibers oriented  $90^\circ$  with respect to

longitudinal direction were included; 4) Test specimens with internal steel reinforcements were excluded; 5) Test specimens failed prematurely due to FRP debonding were excluded; 6) Data from experiments with insufficient documented details i.e. material and geometry properties were excluded; 7) Data from experiments that did not report the axial stress versus axial strain curves (only include the results regarding the ultimate condition) were excluded; 8) Test specimens confined based on a hybrid confinement strategy (simultaneous application of two or more different types of FRP material) were excluded.

In the assembled database, concrete compressive strength ( $f_{c0}$ ) varies from 12.4 to 171 MPa with the mean and CoV values of 37.7 MPa and 0.55, respectively. The diameter of the equivalent circular cross-section ( $D_{eq}$ ) is in the range of 70–318 mm with mean and CoV of 166 mm and 0.26, respectively. The database includes specimens confined with glass (GFRP), basalt (BFRP), aramid (AFRP) and carbon (CFRP). FRP modulus elasticity ( $E_f$ ) varies from 13.6 to 276 GPa with the mean and CoV values of 184.3 MPa and 0.435, respectively, with ultimate tensile strain ( $\epsilon_{fu}$ ) ranging 0.013 – 0.035 with mean and CoV of 0.018 and 0.226, respectively. Confinement stiffness index ( $\rho_{k,f}$ ) varies from 0.01 to 0.262 % with the mean and CoV values as 0.026 % and 1.12, respectively.

It is well-known that the limitation of the conducted model would be dependent on the range of key parameters supported by the assembled database. Consequently, a more reliable regression-based model might be conducted when a larger database covering various ranges of the model parameters is available. Accordingly, by providing a larger database than that used in the present study (Appendix A), the key parameters i.e.  $R_1$  and  $R_2$  in Eqs. (54, 55) can be recalibrated, leading to an improvement in the accuracy of the model. The applicability of the developed model is limited to fully/partially FRP confined circular/square concrete columns and it is not applicable to the case of FRP confined rectangular reinforced concrete (RC) columns where the substantial effects of sectional aspect ratio and internal steel reinforcements in confinement-induced improvements need to be addressed. Nonetheless, the methodology demonstrated in the present study can be extended potentially to FRP confined rectangular RC columns, which will be the focus of a future publication.

## 8. Calculation methodology

In this section, the calculation procedure of the proposed analysis-oriented model to determine global axial stress versus axial strain of FFCC, FPCC, FFSC and FPSC is presented. Considering a FRP confined concrete with a square cross-section ( $R_b$ ) and partial confining config-

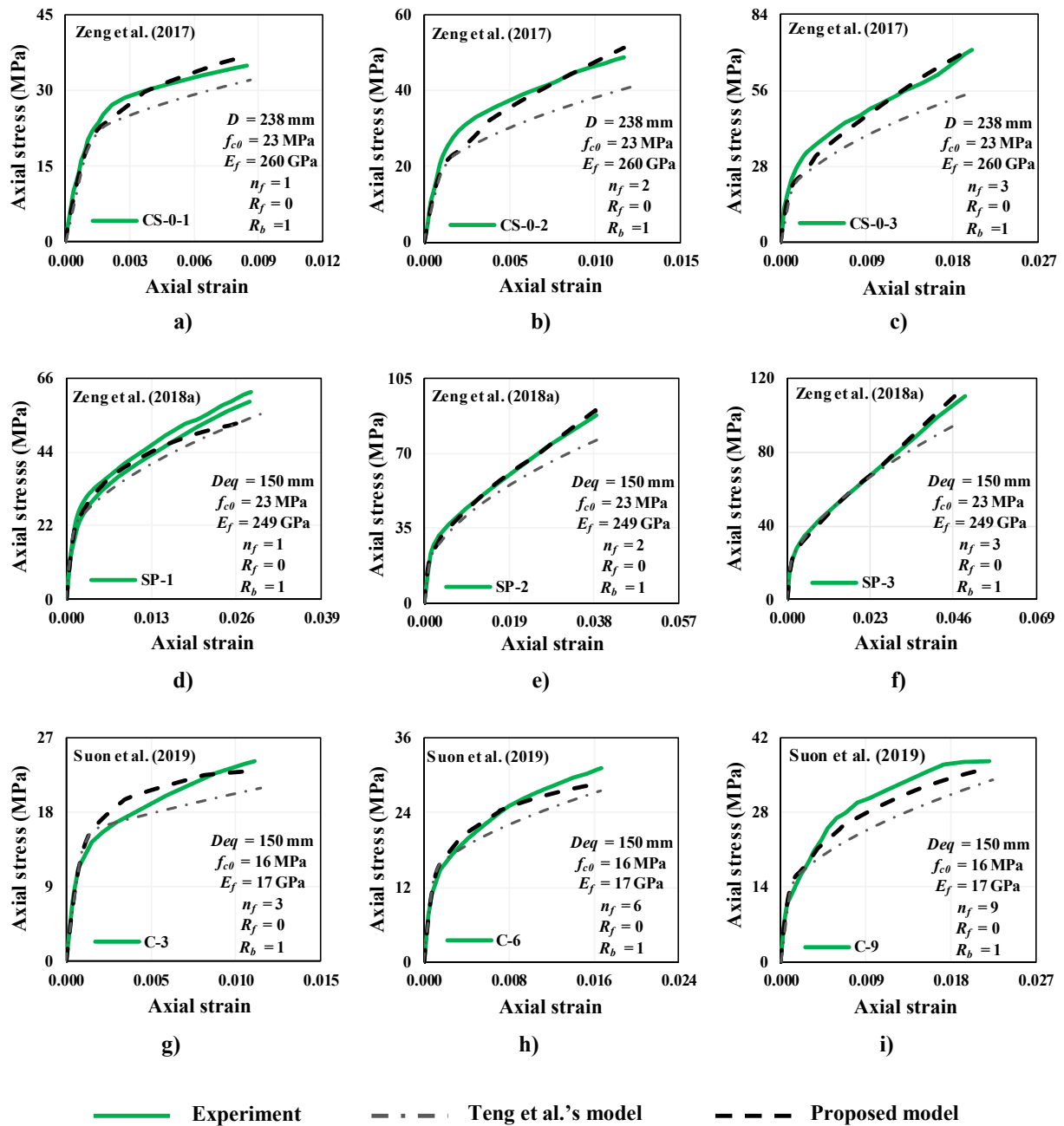


Fig. 14. Analytical simulations versus experimental results reported by Zeng *et al.* [3,14] and Suon *et al.* [8] for FFCC.

uration ( $R_f$ ), the incremental calculation procedure is as follows:

1. Calculate the confinement efficiency factor at horizontal direction  $K_H$  using Eq. (23)
2. Calculate the confinement efficiency factor at vertical direction  $K_V$  using Eq. (43)
3. Calculate the confinement efficiency factor  $K_e$  using Eq. (44)
4. Calculate the confinement stiffness index  $\rho_{Kf}$  using Eq. (49)
5. Assume a value of  $\epsilon_c$
6. Calculate the secant Poisson's ratio  $\nu_s$  using Eq. (50) and the data in Fig. 12
7. Calculate the peak axial stress  $f_{cc}$  using Eq. (48)
8. Calculate the peak axial strain  $\epsilon_{cc}$  using Eq. (46)
9. Calculate the corresponding axial stress  $f_c$  using Eq. (45)
10. Continue the steps 5–9 up to ultimate axial strain

It should be noted in the present study, since the focus of the current study was given on the simulation of global axial stress–strain curves, the experimental ultimate axial strain was adopted to terminate the calculation process.

### 9. Comparison of model predictions with experimental results

This section examines the reliability of the proposed confinement model in the calculation of the axial stress versus axial strain relationship. For this purpose, the axial responses obtained from the experimental axial compressive tests of FFCC, FPCC, FFSC and FPSC were compared with those simulated by the model. The predictive performance was also compared to that of the analysis-oriented model developed by Teng *et al.* [16], with a wide reputation in the relative literature, (originally suggested for FFCC), with implementing some modifications to generalize this model for the case of circular/square



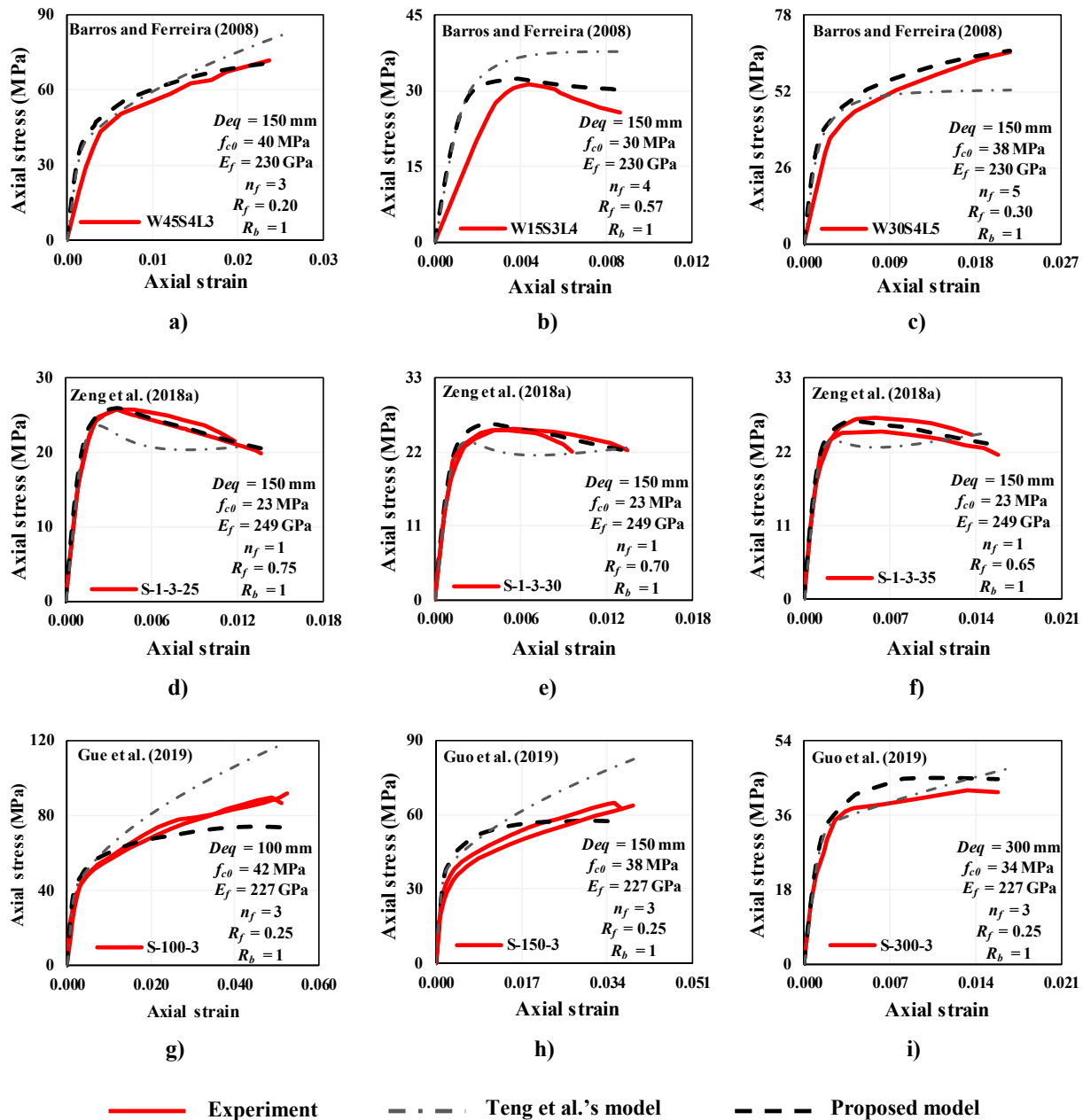


Fig. 15. Analytical simulations versus experimental results reported by Barros and Ferreira [4], Zeng et al. [3] and Guo et al. [5] for FPCC.

cross-section column with full/partial confinement arrangements. This model was briefly presented in Appendix B.

For the case of FFCC, in Fig. 14, the axial capacity curves resulted from the proposed confinement model and Teng et al. [16]’s model are compared with the experimental counterparts conducted by Zeng et al. [3,14] and Suon et al. [8]. As can be seen in Fig. 14a-c, the proposed model and Teng et al. [16]’s model presented almost the same predictive performance up to transition zone, which slightly underestimate the experimental counterparts. However, beyond this stage, the proposed model provided closer predictions with sufficient accuracy. In Fig. 14d-f, the proposed model was capable of closely simulating the full range of the experimental axial stress–strain curves, except for a slight underestimation associated with the ultimate loading stage of the test specimen SP-1 (Fig. 14d). Nonetheless, conservative predictions were given by Teng et al. [16]’s model. For the cases of the test results reported by Suon et al. [8], there is a better predictive performance for the proposed model compared to Teng et al. [16]’s model as demonstrated in Fig. 14g-i. For

the case of the test specimen C-3 (Fig. 14g), even though the proposed model overestimated the experimental axial response between transition and ultimate stages, it has a good accuracy in the estimation of maximum axial compressive strength corresponding to ultimate strain. From Fig. 14, it can be concluded that the proposed model is able to predict with high accuracy the global axial stress–strain curves of the tested circular cross-section specimens with FRP full confinement arrangements. Furthermore, slight conservative results were achieved from Teng et al. [16]’s model in simulating the axial response of the tested specimens.

For the case of FPCC, the test results conducted by Barros and Ferreira [4], Zeng et al. [3] and Guo et al. [5] were simulated by the generalized Teng et al. model [16] (Appendix B) and the proposed confinement model, as illustrated in Fig. 15. As can be seen in Fig. 15a-c, in general, the proposed model could sufficiently estimate the full range of the experimental axial stress–strain curves, even though the initial axial stiffness was higher than that of the experimental counterparts.

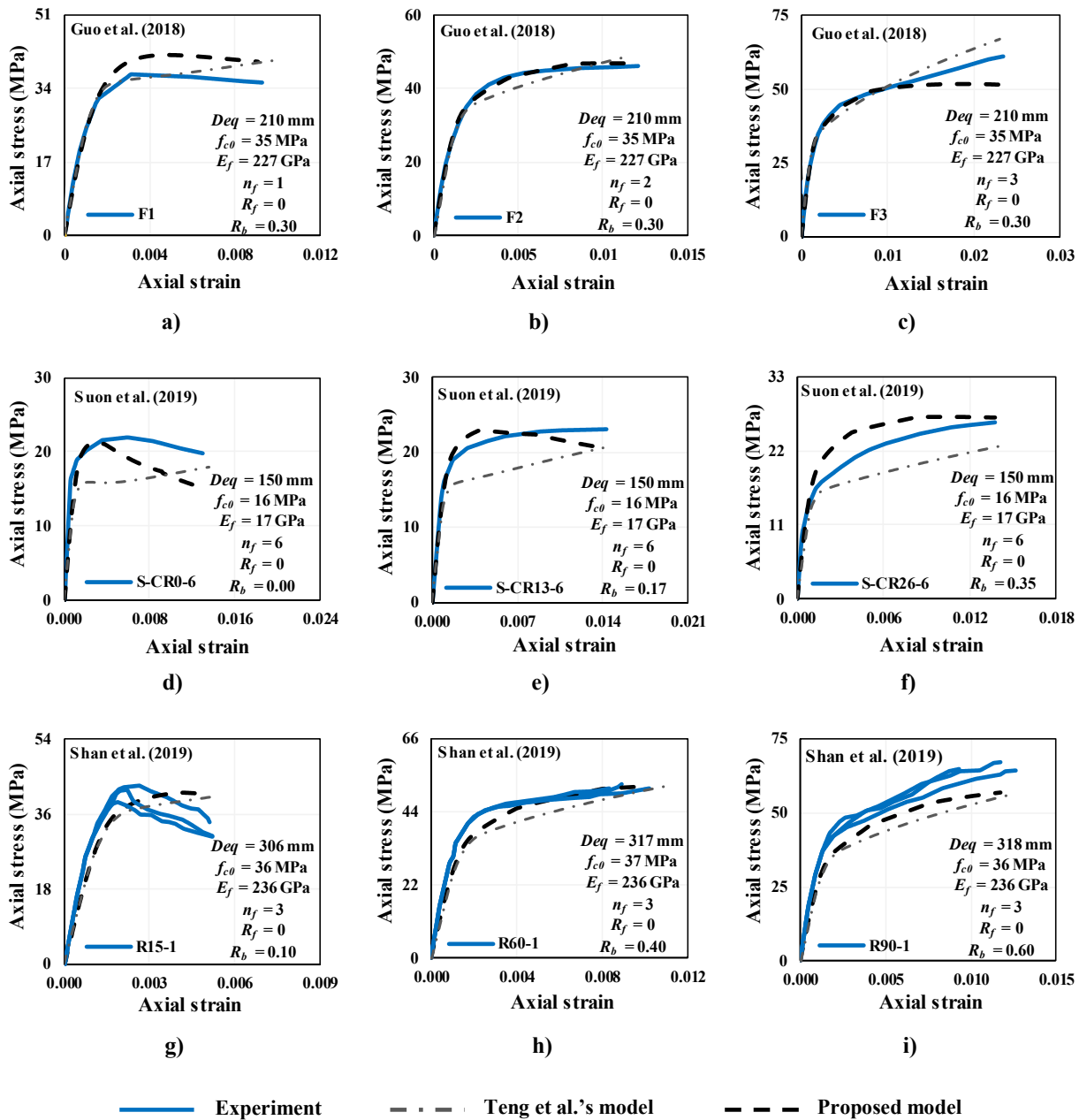


Fig. 16. Analytical simulations versus experimental results reported by Guo et al. [29], Suon et al. [8] and Shan et al. [10] for FFSC.

However, the generalized Teng et al. [16]’s model could not predict sufficiently the experimental axial response. For the cases of the test results reported by Zeng et al. [3], the proposed model presented an excellent prediction accuracy of the test specimens with a relatively large distance between FRP strips (large  $s_f$ ). Even though the generalized Teng et al. [16]’s model could estimate accurately the experimental ultimate axial strength, it was not able to simulate the global axial response as well as maximum axial strength. In Fig. 15a-c, in general, the proposed model has a better predictive performance compared to Teng et al. [16]’s model. The results demonstrated in Fig. 15 can reasonably confirm the assumptions conducted by proposed model for formulating the substantial effect of key parameter of  $s_f$  in terms of the confinement mechanism and confinement -induced improvements of FPCC can be confirmed.

Fig. 16 compares the axial response of the square cross-section columns with full confinement arrangements (FFSC) obtained from the proposed analytical model and the generalized Teng et al. [16]’s model

with the experimental results reported by Guo et al. [29], Suon et al. [8] and Shan et al. [10]. For the case of the test specimen F1 (Fig. 16a), the generalized Teng et al. [16]’s model presented a better predictive performance compared to the proposed model, even though the both models led to an identical maximum compressive strength. However, for the cases of the test specimens F2 and F3, the axial behavior estimated by the proposed model is in an acceptable agreement with the experimental counterparts. As can be seen in Fig. 16d-f, in general, the proposed model demonstrated sufficient capability in estimating the experimental axial response. Although the global axial behavior of the test specimen S-CR26-6 (Fig. 16f) was overestimated by the proposed model, a good estimation was achieved in terms of maximum compressive strength. Nonetheless, the generalized Teng et al. [16]’s model provided significant underestimations of the experimental counterparts. As can be seen in Fig. 16g-i, a slight better predictive performance with sufficient accuracy was demonstrated by the proposed model compared to the generalized Teng et al. [16]’s model. As a result,

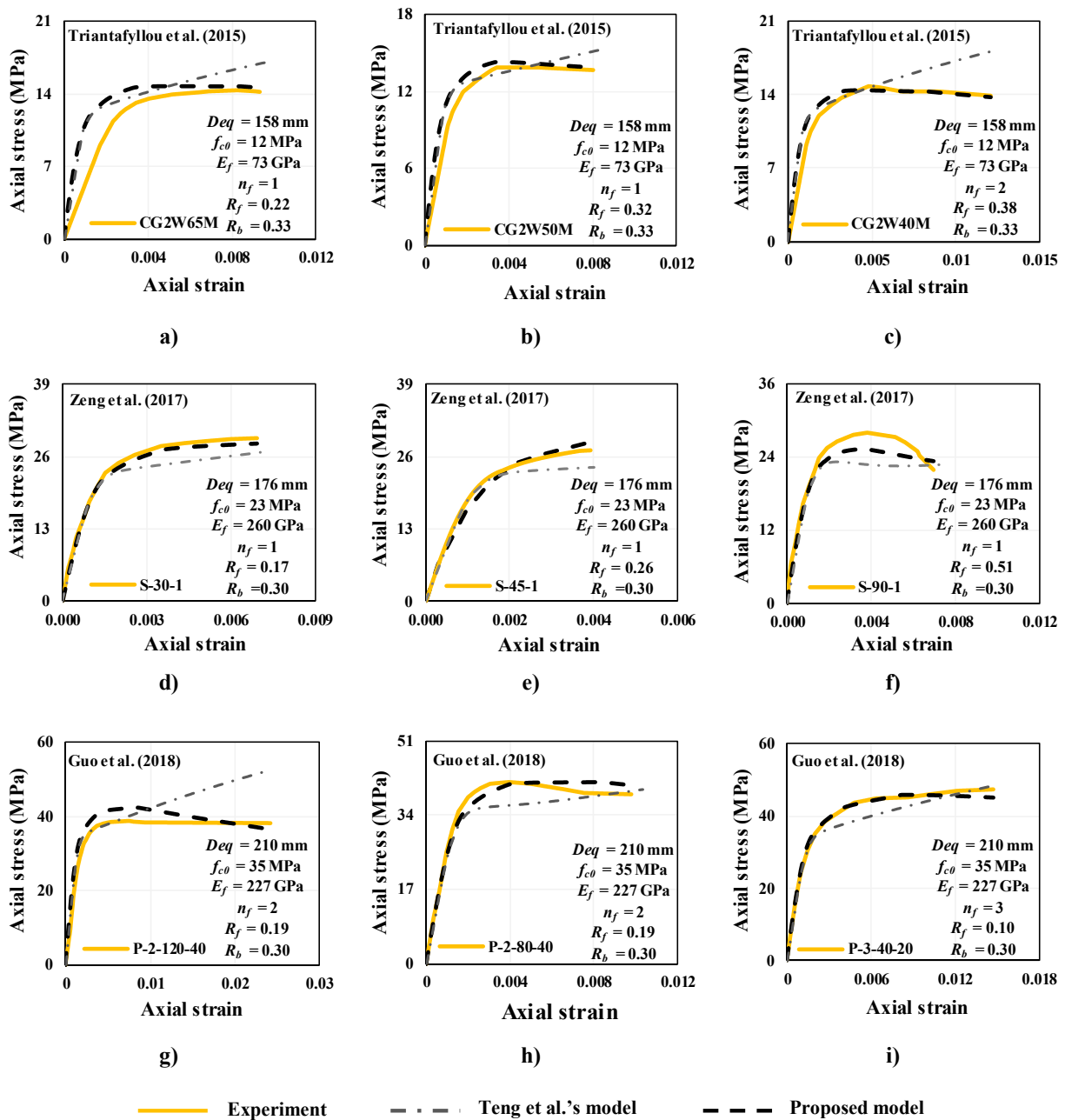


Fig. 17. Analytical simulations versus experimental results reported by Triantafyllou *et al.* [13], Zeng *et al.* [14] and Guo *et al.* [29] for FPSC.

Fig. 16 confirms the reliability of the proposed model in the establishment of the shape effect of square cross-section, with a unified character with FFCC and FPCC, on FRP confinement mechanism, strongly dependent on the dimension of the corner radius  $r$ , in terms of the axial stress versus axial strain relationship.

For the case of FPSC, Fig. 17 compares the axial capacity curves resulted from the proposed model and the generalized Teng *et al.* [16]'s model with the experimental results reported by Triantafyllou *et al.* [13], Zeng *et al.* [14] and Guo *et al.* [29]. As can be seen in Fig. 17a-c, both confinement models generally over-predicted the initial axial stiffness. However, the proposed model could well simulate the full range of the axial stress versus axial strain obtained from Triantafyllou *et al.* [13]. The evaluation of the generalized Teng *et al.* [16]'s model revealed

consistent over-predictions in terms of axial strength capacity. For the case of the test results reported by Zeng *et al.* [14], there is a better predictive performance for the proposed model compared to the generalized Teng *et al.* [16]'s model, which consistently underestimated the experimental counterparts (Fig. 17g-i). As can be seen in Fig. 16g-i, despite a slight overestimation corresponding to the transition zone for the case of P-2-120-40, the proposed model could correctly predict the experimental axial response of FPSC, with a better estimation compared to the generalized Teng *et al.* [16]'s model.

Ultimately, the results provided in Figs. 14-17 reasonably validate the wide applicability of the proposed model for accurately predicting the axial response of FRP confined concrete column with a broad range of material properties and main model parameters associated with

different confining strategies (full and partial system) and the cross-section shapes as square and circular columns.

### 10. Summary and conclusion

In the present study, a new unified confinement model for predicting the global axial strain versus stress response of concrete columns of circular and square cross-sections (SC and CC, respectively) confined with full and partial FRP-based arrangements (FF and FP, respectively) was proposed. An equivalent circular cross-section was proposed for the cases of columns of rectangular cross-section (FFSC and FPSC), for the intended purpose of using a unified approach, as an extension of the one applicable to circular cross-section concrete columns (FFCC and FPCC). For formulating the influence of concrete expansion distribution at the horizontal and vertical directions, an extended version of the model recommended by Shayanfar *et al.* [35] was developed. Accordingly, a generalized confinement pressure was introduced to determine the confinement characteristics of FRP confined concrete. Based on an extensive set of experimental results including 418 test specimens, a new unified analysis-oriented model in compliance with the concept of the confinement efficiency factor was proposed to predict axial stress versus axial strain of FFCC, FPCC, FFSC and FPSC. The predictive performance of the developed confinement model was then assessed through analytically simulating experimental results. The comparison between the analytical model and experimental counterparts highlighted that it is capable of estimating the axial response of FRP confined concrete with good accuracy.

### Appendix A

The assembled database for the case of fully and partially FRP confined circular/square concrete can be found in [Table A1](#).

**Table A1**  
Assembled database for FFCC, FPCC, FFSC and FPSC.

ID	Confinement arrangement					$D_{eq}$ (mm)	$f_{co}$ (MPa)	$\rho_{K,f}$ (%)	$R_I$
	Total	FFCC	FPCC	FFSC	FPSC				
Rochette and Labossie're [62]	15	2		13		100–159	40.3–45.1	0.2–4.2	0.28–2.35
Shehata <i>et al.</i> [63]	4	2		2		150–154	23.7–29.8	0.3–6.6	0.75–3.72
Teng and Lam [36]	3	3				152	30.7–32.7	1.8–4.7	3.15–3.82
Lam and Teng [15]	8			8		155–158	22.6–39.1	0.3–4.1	0.37–4.18
Xiao and Wu [49]	39	39				152	33.7–57.0	1.4–9.3	0.62–3.81
Masia <i>et al.</i> [64]	6			6		106–158	23.0–25.8	1.3–3.6	1.55–2.98
Berthet <i>et al.</i> [50]	15	15				70–160	23.6–171	3.2–15.1	1.10–5.21
Harajli <i>et al.</i> [51]	3			3		137	18.6	0.5–2.3	1.12–2.95
Rousakis <i>et al.</i> [65]	12			12		210	33.0	0.2–1.7	0.37–1.68
Tao <i>et al.</i> [11]	6			6		154–159	21.4–48.1	0.3–3.5	0.37–3.03
Barros and Ferreira [4]	39	8	31			150	18.1–40.0	0.1–26.2	0.18–4.86
Wang and Wu [9]	24	4		20		150–159	30.7–54.1	0.1–5.9	0.08–2.98
Eid <i>et al.</i> [2]	18	18				152	32.1–67.7	0.7–6.9	0.71–3.47
Wu and Wei [40]	2			2		158	35.3	0.6–1.5	0.57–1.72
Benzaid and Mesbah [66]	6	6				160	25.9–61.8	1.0–9.2	0.72–4.10
Lim and Ozbakkaloglu [26]	36	36				152	29.6–98.0	1.0–5.3	1.02–3.46
Triantafyllou <i>et al.</i> [13]	4			1	3	158	12.4	0.1–0.3	0.21–0.63
Vincent and Ozbakkaloglu [67]	6	6				152	110.3	2.7–4.8	1.16–1.73
Zeng <i>et al.</i> [14]	20	3	9	2	6	176–238	22.7–22.9	0.1–8.9	0.27–4.16
Zeng <i>et al.</i> [3]	60	6	54			150	23.4	3.9–13.0	3.18–4.25
Zeng <i>et al.</i> [34]	15		15			150	23.5	0.1–3.8	0.19–2.07
Wang <i>et al.</i> [54]	7	1	6			100	35.9	0.1–5.7	0.17–4.35
Guo <i>et al.</i> [29]	16			3	13	210	34.7	0.1–1.2	0.17–1.42
Guo <i>et al.</i> [5]	21		21			100–300	33.6–41.7	0.2–3.6	0.28–2.61
Suon <i>et al.</i> [8]	12	3		9		150–158	15.6–16.0	0.04–3.8	0.18–3.25
Shan <i>et al.</i> [10]	21	3		18		300–318	35.8–37.2	0.1–3.8	0.1–3.25
ALL	418	155	136	105	22	166 <sup>a</sup> -0.26 <sup>b</sup>	37.7–0.55	2.6–1.12	1.66–0.69

Note: a: Mean; b: CoV.

### 11. Data availability statement

All data and models related to the present study could be available from the corresponding author upon rational request.

#### CRediT authorship contribution statement

**Javad Shayanfar:** Conceptualization, Methodology, Data curation, Validation, Writing – original draft. **Joaquim A. Barros:** Conceptualization, Methodology, Writing – review & editing, Supervision. **Mohammadali Rezazadeh:** Conceptualization, Methodology, Writing – review & editing, Supervision.

#### Declaration of Competing Interest

The authors declare that they have no known competing financial interests or personal relationships that could have appeared to influence the work reported in this paper.

#### Acknowledgements

This study is a part of the project “StreColesf Innovative technique using effectively composite materials for the strengthening of rectangular cross-section reinforced concrete columns exposed to seismic loadings and fire”, with the reference POCI-01-0145-FEDER-029485. The first author also acknowledges the support provided by FCT PhD individual fellowship 2019 with the reference of “SFRH/BD/148002/2019”.

## Appendix B

To determine axial stress versus axial strain curves, Teng *et al.* [16] proposed an analysis-oriented model based on active confinement approach, originally suggested for FFCC. By adopting OCCEF (Mander *et al.* [28]) presented in this study, at a known value of concrete lateral strain ( $\varepsilon_{lj}$ ), the corresponding confinement pressure ( $f_{lf}$ ) imposed on FPSC with the equivalent circular cross-section ( $D_{eq}$ ) can be calculated as:

$$f_{lf} = 2K_e \frac{n_f t_f w_f}{D_{eq}(s_f + w_f)} E_f \varepsilon_{lj} \quad (B1)$$

in which

$$K_e = K_H K_V \quad (B2)$$

$$K_H = 1 - \frac{2(b-2r)^2}{3A_g} \quad (B3)$$

$$K_V = \left(1 - \frac{s_f}{2b}\right)^2 \quad (B4)$$

$$D_{eq} = \sqrt{2}(b-2r) + 2r \quad (B5)$$

$$A_g = b^2 - 4\left(r^2 - \frac{\pi r^2}{4}\right) \quad (B6)$$

Subsequently, the corresponding axial strain ( $\varepsilon_c$ ) can be obtained through a lateral to-axial strain relation as:

$$\frac{\varepsilon_c}{\varepsilon_{c0}} = 0.85 \left[ \left(1 + 0.75 \left(\frac{-\varepsilon_{lj}}{\varepsilon_{c0}}\right)^{0.7} - \exp\left(-7\left(\frac{-\varepsilon_{lj}}{\varepsilon_{c0}}\right)\right)\right) \times \left[1 + 8\left(\frac{f_{lf}}{f_{c0}}\right)\right] \right] \quad (B7)$$

The corresponding axial stress can be predicted as:

$$f_c = f_{cc} \frac{(\varepsilon_c/\varepsilon_{cc})^n}{n-1 + (\varepsilon_c/\varepsilon_{cc})^n} \quad (B8)$$

in which

$$\frac{f_{cc}}{f_{c0}} = 1 + 3.5 \frac{f_{lf}}{f_{c0}} \quad (B9)$$

$$\frac{\varepsilon_{cc}}{\varepsilon_{c0}} = 1 + 17.5 \frac{f_{lf}}{f_{c0}} \quad (B10)$$

$$n = \frac{E_c}{E_c - f_{cc}/\varepsilon_{cc}} \quad (B11)$$

$$\varepsilon_{c0} = 0.000937 f_{c0}^{0.25} \quad (B12)$$

where  $\varepsilon_{cc}$  is the axial strain corresponding to peak axial stress point  $f_{cc}$ ;  $n$  is the concrete brittleness;  $E_c$  is the modulus elasticity of concrete. By repeating the described procedure for a range of  $\varepsilon_{lj}$ ,  $f_c$  versus  $\varepsilon_c$  curve can be obtained.

## References

- [1] Campione G, La Mendola L, Monaco A, Valenza A, Fiore V. Behavior in compression of concrete cylinders externally wrapped with basalt fibers. *Compos Part B Eng* 2015;69:576–86.
- [2] Eid R, Roy N, Paultre P. Normal-and high-strength concrete circular elements wrapped with FRP composites. *J Compos Constr* 2009;13(2):113–24.
- [3] Zeng JJ, Guo YC, Gao WY, Chen WP, Li LJ. Stress-strain behavior of concrete in circular concrete columns partially wrapped with FRP strips. *Compos Struct* 2018; 200:810–28.
- [4] Barros JA, Ferreira DR. Assessing the efficiency of CFRP discrete confinement systems for concrete cylinders. *J Compos Constr* 2008;12(2):134–48.
- [5] Guo YC, Gao WY, Zeng JJ, Duan ZJ, Ni XY, Peng KD. Compressive behavior of FRP ring-confined concrete in circular columns: Effects of specimen size and a new design-oriented stress-strain model. *Constr Build Mater* 2019;201:350–68.
- [6] Ozbakkaloglu T. Behavior of square and rectangular ultra high-strength concrete-filled FRP tubes under axial compression. *Compos Part B Eng* 2013;54:97–111.
- [7] Chen L, Ozbakkaloglu T. Corner strengthening of square and rectangular concrete-filled FRP tubes. *Eng Struct* 2016;117:486–95.
- [8] Suon S, Saleem S, Pimanmas A. Compressive behavior of basalt FRP-confined circular and non-circular concrete specimens. *Constr Build Mater* 2019;19:85–103.
- [9] Wang LM, Wu YF. Effect of corner radius on the performance of CFRP-confined square concrete columns: Test. *Eng Struct* 2008;30(2):493–505.
- [10] Shan B, Gui FC, Monti G, Xiao Y (2019). Effectiveness of CFRP confinement and compressive strength of square concrete columns. *J Compos Constr* 2019 23(6): 04019043.
- [11] Tao Z, Yu Q, Zhong YZ. Compressive behavior of CFRP-confined rectangular concrete columns. *Mag Concr Res* 2008;60(10):735–45.
- [12] Saleem S, Hussain Q, Pimanmas A. Compressive behavior of PET FRP-confined circular, square, and rectangular concrete columns. *J Compos Constr* 2017;21(3): 04016097.
- [13] Triantafillou GG, Rousakis TC, Karabinis AI. Axially loaded reinforced concrete columns with a square section partially confined by light GFRP straps. *J Compos Constr* 2015;19(1):04014035.
- [14] Zeng JJ, Guo YC, Gao WY, Li JZ, Xie JH. Behavior of partially and fully FRP confined circularized square columns under axial compression. *Constr Build Mater* 2017;152:319–32.
- [15] Lam L, Teng JG. Design-oriented stress-strain model for FRP-confined concrete in rectangular columns. *J Reinf Plast Compos* 2003;22(13):1149–86.
- [16] Teng J, Huang YL, Lam L, Ye LP. Theoretical model for fiber-reinforced polymer-confined concrete. *J Compos Constr* 2007;11(2):201–10.
- [17] Teng JG, Jiang T, Lam L, Luo YZ. Refinement of a design-oriented stress-strain model for FRP-confined concrete. *J Compos Constr* 2010;13(4):269–78.
- [18] Lee CS, Hegemier GA, Phillippi DJ. Analytical model for fiber-reinforced polymer-jacketed square concrete columns in axial compression. *ACI Struct J* 2010;107(2): 208.
- [19] Lim JC, Ozbakkaloglu T. Lateral strain-to-axial strain relationship of confined concrete. *J Struct Eng* 2014;141(5):04014141.
- [20] Lim JC, Ozbakkaloglu T. Unified stress-strain model for FRP and actively confined normal strength and high-strength concrete. *J Compos Constr* 2014;19(4): 04014072.
- [21] Moran DA, Pantelides CP, Reaveley LD. Mohr-coulomb model for rectangular and square FRP-confined concrete. *Compos Struct* 2019;209:889–904.

- [22] Yang JQ, Feng P. Analysis-oriented models for FRP-confined concrete: 3D interpretation and general methodology. *Eng Struct* 2020;216:110749.
- [23] Lin S, Zhao YG, Li J, Lu ZH. Confining stress path-based compressive strength model of axially loaded FRP-confined columns. *J Compos Constr* 2020;25(1):04020077.
- [24] Lin G, Teng JG. Advanced stress-strain model for FRP-confined concrete in square columns. *Compos Part B Eng* 2020;197:108149.
- [25] Popovics S. A numerical approach to the complete stress-strain curve of concrete. *Cem Concr Res* 1973;3(5):583–99.
- [26] Lim JC, Ozbakkaloglu T. Hoop strains in FRP-confined concrete columns: experimental observations. *Mater Struct* 2014;48(9):2839–54.
- [27] Lim JC, Ozbakkaloglu T. Stress-strain model for normal-and light-weight concretes under uniaxial and triaxial compression. *Constr Build Mater* 2014;71:492–509.
- [28] Mander JB, Priestley MJ, Park R. Theoretical stress-strain model for confined concrete. *J Struct Eng* 1988;114(8):1804–26.
- [29] Guo YC, Xiao SH, Luo JW, Ye YY, Zeng JJ. Confined Concrete in Fiber-Reinforced Polymer Partially Wrapped Square Columns: Axial Compressive Behavior and Strain Distributions by a Particle Image Velocimetry Sensing Technique. *Sensors* 2018;18(12):4118.
- [30] Mostofinejad D, Ilia E, Mortazavi N. Fibre-reinforced polymer efficiency in square columns with different corner radii. *Proceedings of the Institution of Civil Engineers-Structures and Buildings* 2018;171(3):241–52.
- [31] Minafo G, Rezaee-Hajidehi M, Giambanco. A Mechanical Approach for Evaluating the Distribution of Confinement Pressure in FRP-Wrapped Rectangular Columns. *Journal of Engineering Mechanics* 2019;145(12):04019092.
- [32] Jiang J, Li P, Nisticò N. Local and global prediction on stress-strain behavior of FRP-confined square concrete sections. *Compos Struct* 2019;226:111205.
- [33] Oliveira D, Carrazedo R. Numerical modeling of circular, square and rectangular concrete columns wrapped with FRP under concentric and eccentric load. *Revista IBRACON de Estruturas e Materiais* 2019;12(3):518–50.
- [34] Zeng J, Guo Y, Li L, Chen W. Behavior and three-dimensional finite element modeling of circular concrete columns partially wrapped with FRP strips. *Polymers* 2018;10(3):253.
- [35] Shayanfar J, Rezaadeh M, Barros JA. Analytical model to predict dilation behavior of FRP confined circular concrete columns subjected to axial compressive loading. *J Compos Constr* 2020;24(6):04020071.
- [36] Teng JG, Lam L. Compressive behavior of carbon fiber reinforced polymer-confined concrete in elliptical columns. *J Struct Eng* 2002;128(12):1535–43.
- [37] Teng JG, Wu JY, Casalboni S, Xiao QG, Zhao Y. Behavior and modeling of fiber-reinforced polymer-confined concrete in elliptical columns. *Adv Struct Eng* 2016;19(9):1359–78.
- [38] Triantafyllou TC, Choutopoulou E, Fotaki E, Skorda M, Stathopoulou M, Karlos K. FRP confinement of wall-like reinforced concrete columns. *Mater Struct* 2016;49(1–2):651–64.
- [39] Zhu JY, Lin G, Teng JG, Chan TM, Zeng JJ, Li LJ. FRP-confined square concrete columns with section curvilinearization under axial compression. *J Compos Constr* 2020;24(2):04020004.
- [40] Wu YF, Wei YY. Effect of cross-sectional aspect ratio on the strength of CFRP-confined rectangular concrete columns. *Eng Struct* 2010;32(1):32–45.
- [41] Pantelides CP, Yan Z, Reaveley LD. Shape modification of rectangular columns confined with FRP composites. Report No. UT-05.03, Utah Department of Transportation Research and Development Division 2004.
- [42] Wang Z, Wang D, Smith ST, Lu D. CFRP-confined square RC columns. I: Experimental investigation. *J Compos Constr* 2012;16(2):150–60. 21.
- [43] Xiaojie L, Xiaolei H, Jing J, Zhengrong J, Binbin C. Axial Compression Behavior of CFRP-confined Damaged Reinforced Concrete. *JSCUT (Natural Science Edition)* 2019;47(7):1–9 (in Chinese).
- [44] Wang DY, Wang ZY, Smith ST. Size effect on axial stress-strain behavior of CFRP-confined square concrete columns. *Constr Build Mater* 2016;118:116–26.
- [45] Wei Y, Wu YF. Experimental study of concrete columns with localized failure. *J Compos Constr* 2016;20(5):04016032.
- [46] Fallahpour A, Nguyen GD, Vincent T, Ozbakkaloglu T. Investigation of the compressive behavior and failure modes of unconfined and FRP-confined concrete using digital image correlation. *Compos Struct* 2020;252:112642.
- [47] Wu YF, Wei Y. Stress-Strain Modeling of Concrete Columns with Localized Failure: An Analytical Study. *J Compos Constr* 2016;20(3):04015071.
- [48] Mirmiran A, Shahawy M. Dilation characteristics of confined concrete. *Mechanics of Cohesive- frictional Materials: Mech Cohesive-Frict Mater* 1997;2(3):237–49.
- [49] Xiao Y, Wu H. Compressive behavior of concrete confined by various types of FRP composite jackets. *J Reinforc Plast Compos* 2003;22(13):1187–201.
- [50] Berthet JF, Ferrier E, Hamelin P. Compressive behavior of concrete externally confined by composite jackets. Part A: experimental study. *Constr Build Mater* 2005;19(3):223–32.
- [51] Harajli MH, Hantouche E, Soudki K. Stress-strain model for fiber-reinforced polymer jacketed concrete columns. *Structural Journal* 2006;103(5):672–82.
- [52] Shayanfar J, Rezaadeh M, Barros JA, Ramezansafat H. A new dilation model for FRP fully/partially confined concrete column under axial loading. *Guimarães Portugal: Comprehensive Strategies for Unprecedented Challenges*; 2020.
- [53] Shayanfar J, Barros JA, Rezaadeh M. Generalized analysis-oriented model of FRP confined concrete circular columns. *Compos Struct* 2021;270:114026.
- [54] Wang W, Sheikh MN, Al-Baali AQ, Hadi MN. Compressive behaviour of partially FRP confined concrete: Experimental observations and assessment of the stress-strain models. *Constr Build Mater* 2018;192:785–97.
- [55] Lertsrisakulrat T, Watanabe K, Matsuo M, Niwa J. Experimental study on parameters in localization of concrete subjected to compression. *J Mater Concr Struct Pavements* 2001;50(669):309–21.
- [56] Carreira and Chu (1985). Stress-strain relationship for plain concrete in compression. In *Journal Proceedings* 1985;82(6):797–804.
- [57] ACI 318M–08. Building code requirements for reinforced concrete. Detroit (Michigan): American Concrete Institute; 2008.
- [58] Candappa DC, Sanjayan JG, Setunge S. Complete triaxial stress-strain curves of high-strength concrete. *J Mater Civ Eng* 2001;13(3):209–15.
- [59] Kwan AKH, Dong CX, Ho JCM. Axial and lateral stress-strain model for FRP confined concrete. *Eng Struct* 2015;99:285–95.
- [60] Ho JCM, Ou XL, Chen MT, Wang Q, Lai MH. A path dependent constitutive model for CFFT column. *Eng Struct* 2020;210:110367.
- [61] Lai MH, Liang YW, Wang Q, Ren FM, Chen MT, Ho JCM. A stress-path dependent stress strain model for FRP-confined concrete. *Eng Struct* 2020;203:109824.
- [62] Rochette P, Labossiere P. Axial testing of rectangular column models confined with composites. *J Compos Constr* 2000;4(3):129–36.
- [63] Shehata IA, Carneiro LA, Shehata LC. Strength of short concrete columns confined with CFRP sheets. *Mater Struct* 2002;35(1):50–8.
- [64] Masia MJ, Gale TN, Shrive NG. Size effects in axially loaded square-section concrete prisms strengthened using carbon fiber reinforced polymer wrapping. *Can J Civ Eng* 2004;31:1–13.
- [65] Rousakis TC, Karabinis AI, Kioussis PD. FRP-confined concrete members: axial compression experiments and plasticity modelling. *Eng Struct* 2007;29(7):1343–53.
- [66] Benzaid R, Mesbah HA. Circular and square concrete columns externally confined by CFRP composite: experimental investigation and effective strength models. *Fiber Reinforced Polymers-The Technology Applied for Concrete Repair* 2013:167–201.
- [67] Vincent T, Ozbakkaloglu T. Compressive behavior of prestressed high-strength concrete-filled aramid FRP tube columns: Experimental observations. *J Compos Constr* 2015;19(6):04015003.